

Inclusive W and Z production in the forward region at $\sqrt{s} = 7$ TeV



The LHCb collaboration

ABSTRACT: Measurements of inclusive W and Z boson production cross-sections in pp collisions at $\sqrt{s} = 7$ TeV using final states containing muons are presented. The data sample corresponds to an integrated luminosity of 37 pb^{-1} collected with the LHCb detector. The W and Z bosons are reconstructed from muons with a transverse momentum above $20 \text{ GeV}/c$ and pseudorapidity between 2.0 and 4.5, and, in the case of the Z cross-section, a dimuon invariant mass between 60 and $120 \text{ GeV}/c^2$. The cross-sections are measured to be $831 \pm 9 \pm 27 \pm 29 \text{ pb}$ for W^+ , $656 \pm 8 \pm 19 \pm 23$ for W^- and $76.7 \pm 1.7 \pm 3.3 \pm 2.7 \text{ pb}$ for Z , where the first uncertainty is statistical, the second is systematic and the third is due to the luminosity. Differential cross-sections, W and Z cross-section ratios and the lepton charge asymmetry are also measured in the same kinematic region. The ratios are determined to be $\sigma_{W^+ \rightarrow \mu^+ \nu} / \sigma_{W^- \rightarrow \mu^- \bar{\nu}} = 1.27 \pm 0.02 \pm 0.01$ and $(\sigma_{W^+ \rightarrow \mu^+ \nu} + \sigma_{W^- \rightarrow \mu^- \bar{\nu}}) / \sigma_{Z \rightarrow \mu \mu} = 19.4 \pm 0.5 \pm 0.9$. The results are in general agreement with theoretical predictions, performed at next-to-next-to-leading order in QCD using recently calculated parton distribution functions.

KEYWORDS: Hadron-Hadron Scattering

ARXIV EPRINT: [1204.1620](https://arxiv.org/abs/1204.1620)

Contents

1	Introduction	1
2	LHCb detector and Monte Carlo samples	3
3	Selection of W and Z events	4
3.1	Muon reconstruction and identification	4
3.2	Selection of $Z \rightarrow \mu\mu$ candidates	4
3.3	$Z \rightarrow \mu\mu$ event yield	4
3.4	Selection of $W \rightarrow \mu\nu$ candidates	6
3.5	$W \rightarrow \mu\nu$ event yield	9
4	Cross-section measurement	10
4.1	Cross-section definition	10
4.2	Signal efficiencies	10
4.3	Acceptance	13
4.4	Luminosity	13
4.5	Corrections to the data	13
4.6	Systematic uncertainties	13
5	Results	15
6	Conclusions	19
A	Tables of results	21
	The LHCb collaboration	26

1 Introduction

The measurement of the production cross-sections for W and Z bosons constitutes an important test of the Standard Model and provides valuable input to constrain the proton parton density functions (PDFs). Theoretical predictions are known to next-to-next-to-leading-order (NNLO) in perturbative quantum chromodynamics (pQCD). These calculations are in good agreement with recent measurements at the LHC from the ATLAS [1, 2], and the CMS [3, 4] experiments as well as with the results from the $p\bar{p}$ collider experiments at the Sp \bar{p} S [5, 6] and the Tevatron [7–10]. The dominant theoretical uncertainty on the cross-sections arises from the present knowledge of the PDFs and the

strong coupling constant. The accuracy strongly depends on the pseudorapidity¹ range; consequently, measurements by LHCb, which is fully instrumented in the forward region $2.0 < \eta < 5.0$, can provide input to constrain the PDFs, both for pseudorapidities $\eta > 2.5$ and in the region which is common to ATLAS and CMS, $2.0 < \eta < 2.5$. Besides the determination of the W and Z boson cross-sections, the measurement of their ratios $R_{WZ} = (\sigma_{W^+ \rightarrow \mu^+ \nu} + \sigma_{W^- \rightarrow \mu^- \bar{\nu}}) / \sigma_{Z \rightarrow \mu \mu}$ and $R_W = \sigma_{W^+ \rightarrow \mu^+ \nu} / \sigma_{W^- \rightarrow \mu^- \bar{\nu}}$ and of the W production charge asymmetry constitute important tests of the Standard Model, as experimental and theoretical uncertainties partially cancel. The W charge asymmetry is sensitive to the valence quark distribution in the proton [11] and provides complementary information to the results from deep-inelastic scattering cross-sections at HERA [12] as those data do not strongly constrain the ratio of u over d quarks at low Bjorken x , where x is the proton momentum fraction carried by the quark. Measurements of W and Z boson production at LHCb have a sensitivity to values of x as low as 1.7×10^{-4} and will contribute significantly to the understanding of PDFs at low x and reasonably large four-momentum transfer Q^2 , which corresponds to the squared mass of the W or the Z boson.

The measurements of the inclusive W and Z cross-sections² in pp collisions at a centre-of-mass energy of 7 TeV, using final states containing muons, are presented in this paper. The analysis is based on data taken by the LHCb experiment in 2010 with an integrated luminosity of 37 pb^{-1} . The cross-sections are measured in a fiducial region corresponding to the kinematic coverage of the LHCb detector, where the final state muons have a transverse momentum, p_T^μ , exceeding $20 \text{ GeV}/c$ and lie within the pseudorapidity range $2.0 < \eta^\mu < 4.5$. This range is smaller than the LHCb acceptance in order to avoid edge effects for the acceptance. In addition, the invariant mass of the muons from the Z boson must be in the range $60 < M_{\mu\mu} < 120 \text{ GeV}/c^2$. Results are presented for the total cross-sections and cross-section ratios. Cross-sections are also measured in bins of muon pseudorapidity for W , and in bins of Z rapidity (y^Z) for Z production. Because of the presence of the neutrino, the production asymmetry between W^+ and W^- cannot be reconstructed as a function of the boson rapidity. Instead it is measured as a function of the experimentally accessible muon pseudorapidity, η^μ , and referred to as the lepton charge asymmetry $A_\mu = (\sigma_{W^+ \rightarrow \mu^+ \nu} - \sigma_{W^- \rightarrow \mu^- \bar{\nu}}) / (\sigma_{W^+ \rightarrow \mu^+ \nu} + \sigma_{W^- \rightarrow \mu^- \bar{\nu}})$. To constrain the PDFs, it is useful to measure A_μ for different p_T^μ thresholds. The data are compared to NNLO and NLO pQCD predictions with recent parametrisations for the PDFs. The signal efficiency and background contribution are mostly derived from data.

The remainder of the paper is organised as follows. Section 2 describes the LHCb detector and the Monte Carlo samples. Section 3 describes the selection of the W and Z candidates, the backgrounds, the determination of the purity and the signal efficiencies. The measurement of the cross-sections as well as the systematic uncertainties are discussed in section 4. The results are presented in section 5 and conclusions in section 6.

¹The pseudorapidity η is defined to be $\eta = -\ln \tan(\theta/2)$, where the polar angle θ is measured with respect to the beam axis.

²Throughout this paper Z includes both the Z and the virtual photon (γ^*) contribution.

2 LHCb detector and Monte Carlo samples

The LHCb detector [13] is a single-arm forward spectrometer covering the pseudorapidity range $2 < \eta < 5$, designed for the study of particles containing b or c quarks. The detector includes a high precision tracking system consisting of a silicon-strip vertex detector (VELO) surrounding the pp interaction region, a large-area silicon-strip detector (TT) located upstream of a dipole magnet with a bending power of about 4 Tm, and three stations of silicon-strip detectors (IT) and straw drift-tubes (OT) placed downstream. The combined tracking system has a momentum resolution $\Delta p/p$ that varies from 0.4% at 5 GeV/ c to 0.6% at 100 GeV/ c , and an impact parameter (IP) resolution of 20 μm for tracks with high transverse momentum. Charged hadrons are identified using two ring-imaging Cherenkov detectors. Photon, electron and hadron candidates are identified by a calorimeter system consisting of scintillating-pad and pre-shower detectors, an electromagnetic calorimeter and a hadronic calorimeter. Muons are identified by a muon system composed of alternating layers of iron and multiwire proportional chambers. The trigger consists of a hardware stage, based on information from the calorimeter and muon systems, followed by a software stage which applies a full event reconstruction. To avoid the possibility that a few events with high occupancy dominate the CPU time of the software trigger, a set of global event cuts is applied on the hit multiplicities of most subdetectors used in the pattern recognition algorithms.

Several Monte Carlo (MC) simulated samples are used to develop the event selection, estimate the backgrounds, cross-check the efficiencies and to account for the effect of the underlying event. The PYTHIA 6.4 [14] generator, configured as described in ref. [15], with the CTEQ6ll [16] parametrisation for the PDFs is used to simulate the processes $Z \rightarrow \mu\mu$, $Z \rightarrow \tau\tau$, $W \rightarrow \mu\nu$ and $W \rightarrow \tau\nu$. The hard partonic interaction is calculated in leading order pQCD and higher order QCD radiation is modelled using initial and final state parton showers in the leading log approximation [17]. The fragmentation into hadrons is simulated in PYTHIA by the Lund string model [18]. All generated events are passed through a GEANT4 [19] based detector simulation, the trigger emulation and the event reconstruction chain of the LHCb experiment.

Samples of $W \rightarrow \mu\nu$ and $Z \rightarrow \mu\mu$ simulated events with one muon in the LHCb acceptance have been reweighted to reproduce the NNLO p_{T}^{μ} distribution. These samples are referred to as W -MC and Z -MC, respectively. In the first step a correction factor is calculated as a function of the generated muon transverse momentum by determining the ratio of the generated p_{T}^{μ} spectrum, as simulated by the POWHEG [20–22] generator at NLO, to the generated p_{T}^{μ} spectrum from PYTHIA. In the second step the events are reweighted with a factor given by the ratio between the NNLO and NLO prediction as calculated with DNNLO [23]. This factor is calculated as a function of the rapidity of the boson. As an alternative, PYTHIA samples have been reweighted to reproduce the p_{T}^{μ} distribution as calculated with RESBOS [24–26]. RESBOS includes a NLO calculation plus next-to-next-to-leading-log resummation of QCD effects at low transverse momentum.

3 Selection of W and Z events

3.1 Muon reconstruction and identification

Events with high transverse momentum muons are selected using a single muon trigger with a threshold of $p_T^\mu > 10 \text{ GeV}/c$. Tracks are reconstructed starting from the VELO, within which particle trajectories are approximately straight, since the detector is located upstream of the magnet. Candidate tracks are extrapolated to the other side of the magnet and a search is made for compatible hits in the IT and OT sub-detectors. An alternative strategy searches for track segments in both the VELO and IT/OT detectors and extrapolates each to the bending plane of the magnet, where they are matched. Once VELO and IT/OT hits have been combined, an estimate of the track momentum is available and the full trajectory can be defined. Finally, hits in the TT sub-detector are added if consistent with the candidate tracks. Thus, the presence of TT hits can be considered as an independent confirmation of the validity of the track.

Muons are identified by extrapolating the tracks and searching for compatible hits in the four most downstream muon stations. For the high momentum muons that concern this analysis, hits must be found in all four muon stations. In total, the muon candidate must have passed through over 20 hadronic interaction lengths of material.

3.2 Selection of $Z \rightarrow \mu\mu$ candidates

Candidate $Z \rightarrow \mu\mu$ events are selected by requiring a pair of well reconstructed tracks identified as muons; the invariant mass of the two muons must be in the range $60 < M_{\mu\mu} < 120 \text{ GeV}/c^2$. Each muon track must have $p_T^\mu > 20 \text{ GeV}/c$ and lie in the range $2.0 < \eta^\mu < 4.5$. The relative uncertainty on the momentum measurement is required to be less than 10% and the probability for the χ^2/ndf for the track fit larger than 0.1%, where ndf is the number of degrees of freedom. In total, 1966 Z candidates are selected; their mass distribution is shown in figure 1. The data are not corrected for initial or final state radiation. A Crystal Ball [27] function for the Z peak, and an exponential distribution for both the off-resonance Drell-Yan (γ^*) production and the small background contribution are fitted to the distribution. The fitted mass $90.7 \pm 0.1 \text{ GeV}/c^2$ and width $3.0 \pm 0.1 \text{ GeV}/c^2$, where the uncertainties are statistical, are consistent with expectation from simulation.

3.3 $Z \rightarrow \mu\mu$ event yield

The background contribution to the $Z \rightarrow \mu\mu$ analysis is very low. Five different sources are investigated.

1. Decays from $Z \rightarrow \tau\tau$ contribute, if both taus decay leptonically to muons and neutrinos. The tau background is estimated from simulation, with the Z cross-section fixed to the cross-section measured in this analysis, to contribute 0.6 ± 0.1 events to the total sample.
2. Decays of heavy flavour hadrons contribute to the background if they decay semileptonically (“heavy flavour” background). The contribution is estimated from a sample, which is enriched in background. “Non-isolated” muons are selected with $p_T^\mu >$

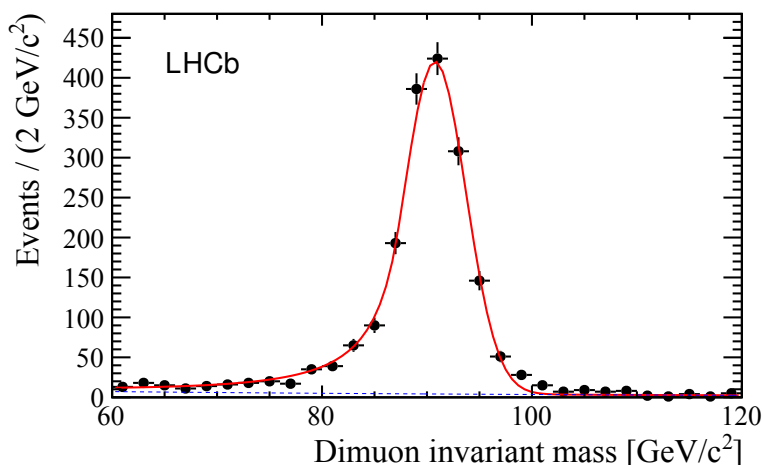


Figure 1. Invariant mass of the selected muon pairs. The fitted distribution to the data is shown as a solid line and the contribution from background and off-resonance Drell-Yan production as a dashed line.

$15 \text{ GeV}/c$ and $M_{\mu\mu} > 40 \text{ GeV}/c^2$ and the scalar sum of the transverse momenta of all tracks in a cone of half angle 0.5 in η - ϕ around the muons larger than $4 \text{ GeV}/c$; here ϕ is the azimuthal angle measured in radians. A fit to the invariant mass distribution at low masses is then used to estimate the background contribution in the Z mass region. The heavy flavour contribution is estimated to be 3.5 ± 0.8 events.

3. Pions or kaons may be misidentified as muons if they decay in flight (“decay-in-flight” background) or if they travel through the calorimeters and are identified by the muon chambers (“punch-through” background). This background should contribute equally in same-sign and opposite-sign combinations of the muon pair. No event is found in the Z selection with both tracks having the same charge. The contribution from muon misidentification is estimated to be less than one event.
4. W pair production contributes to the sample if both W bosons decay to a muon and a neutrino. This contribution corresponds to 0.2 ± 0.1 events as estimated with PYTHIA MC simulation.
5. Decays of top quark pairs may contribute if both top quarks decay semileptonically. PYTHIA MC simulation predicts a contribution of 0.5 ± 0.2 events.

The total background contribution in the Z sample in the range 60 – $120 \text{ GeV}/c^2$ amounts to 4.8 ± 1.0 events. This corresponds to a purity $\rho^Z = 0.997 \pm 0.001$. The purity is defined as the ratio of signal to candidate events. No significant dependence on the boson rapidity is observed.

3.4 Selection of $W \rightarrow \mu\nu$ candidates

In leading order QCD, $W \rightarrow \mu\nu$ events are characterised by a single high transverse momentum muon that is not associated with other activity in the event. As only the muon can be reconstructed in LHCb, the background contribution is larger for the W than for the Z candidates. Therefore, more stringent requirements are placed on the track quality of the muon and additional criteria are imposed in order to select W candidates.

The optimisation of the W selection and the evaluation of the selection efficiency make use of a “pseudo- W ” control sample obtained from the previously described Z selection, where each of the muons is masked in turn, in order to mimic the presence of a neutrino and fake a $W \rightarrow \mu\nu$ decay. Excellent agreement is observed for all variables of interest between pseudo- W and W simulated samples with the exception of those that have an explicit dependence on the transverse momentum of the muon, as the underlying momentum distribution differs for muons from Z and W .

The identification of $W \rightarrow \mu\nu$ candidate events starts by requiring a well reconstructed track which is identified as a muon. The track must have a transverse momentum in the range $20 < p_T^\mu < 70 \text{ GeV}/c$ within a pseudorapidity range $2.0 < \eta^\mu < 4.5$. The relative error on the momentum measurement must be less than 10%, the probability for the χ^2/ndf of the track fit must be greater than 1%, and there must be TT hits associated to the track. The last requirement reduces the number of combinations of VELO and IT/OT information that have been incorrectly combined to form tracks.

To suppress background from $Z \rightarrow \mu\mu$ decays, it is required that any other identified muon in the event has a transverse momentum below $2 \text{ GeV}/c$. This removes the events where both muons have entered the LHCb acceptance.

Identified muons can originate from background processes of heavy flavour decays, or misidentification of pions and kaons due to decay-in-flight or punch-through (“QCD background”). In all such cases, the identified muon is usually produced in the same direction as the other fragmentation products, in contrast to muons from W decays which tend to be isolated. The isolation of the muon is described using the charged transverse momentum, p_T^{cone} , and neutral transverse energy, E_T^{cone} , in a cone around the candidate muon. The quantity p_T^{cone} is defined as the scalar sum of the transverse momentum of all tracks, excluding the candidate muon, satisfying $\sqrt{(\Delta\phi)^2 + (\Delta\eta^\mu)^2} < 0.5$, where $\Delta\phi$ and $\Delta\eta^\mu$ are the differences in ϕ and η between the muon candidate and the track. The quantity E_T^{cone} is defined in a similar way, but summing the transverse energy of all electromagnetic calorimeter deposits not associated with tracks. The distributions for p_T^{cone} and E_T^{cone} are shown in figure 2 for pseudo- W data, W -MC and muons with $p_T^\mu > 20 \text{ GeV}/c$ and an IP larger than $80 \mu\text{m}$. The IP of the muon is defined as the distance of closest approach to the primary vertex calculated from the other tracks in the event excluding the muon candidate. The sample with high IP is enriched with muons from decays of heavy flavour hadrons, showing the typical shape of QCD background. There is agreement between pseudo- W data and W -MC, while the shape for the heavy flavour events is quite different. To suppress QCD background, it is required that $p_T^{\text{cone}} < 2 \text{ GeV}/c$ and $E_T^{\text{cone}} < 2 \text{ GeV}$.

Muons originating from semi-leptonic decays of heavy flavour hadrons can be further suppressed by a cut on the IP. Due to the lifetimes of the B and D mesons, these muons

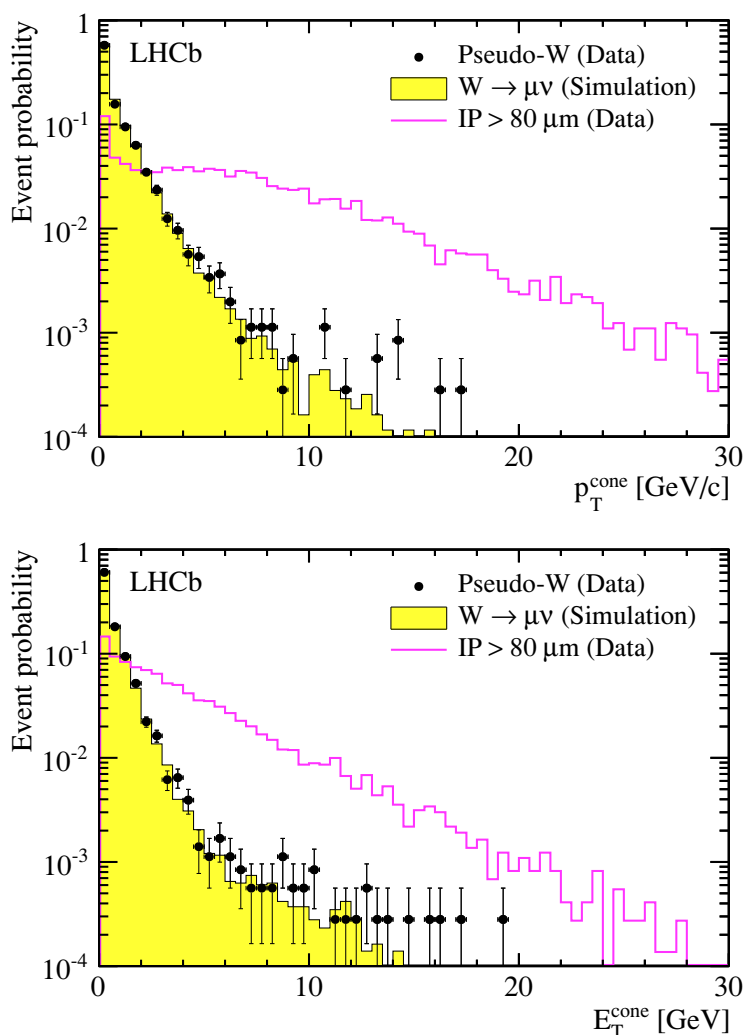


Figure 2. Distributions for p_T^{cone} (top) and E_T^{cone} (bottom). The points are for muons from pseudo- W data, the yellow (shaded) histograms are for W -MC simulation, while the open histograms are for muons from QCD background with $\text{IP} > 80 \mu\text{m}$ from data. All distributions are normalised to unity.

do not originate from the primary pp interaction. The IP distribution is shown in figure 3 for pseudo- W events, W -MC, and simulated semi-leptonic decays of hadrons containing a b or c quark. The pseudo- W events and W -MC are in agreement and peak at low values of IP, in contrast to the heavy flavour background. For the W candidate selection it is required that $\text{IP} < 40 \mu\text{m}$. This cut also removes a large fraction of the background from $W \rightarrow \tau\nu$ and $Z \rightarrow \tau\tau$ decays.

Pions and kaons that punch-through to the muon chambers can be distinguished from true muons as they leave substantial energy deposits in the calorimeters. Figure 4 shows the summed energy, E , in the electromagnetic and hadronic calorimeter associated with

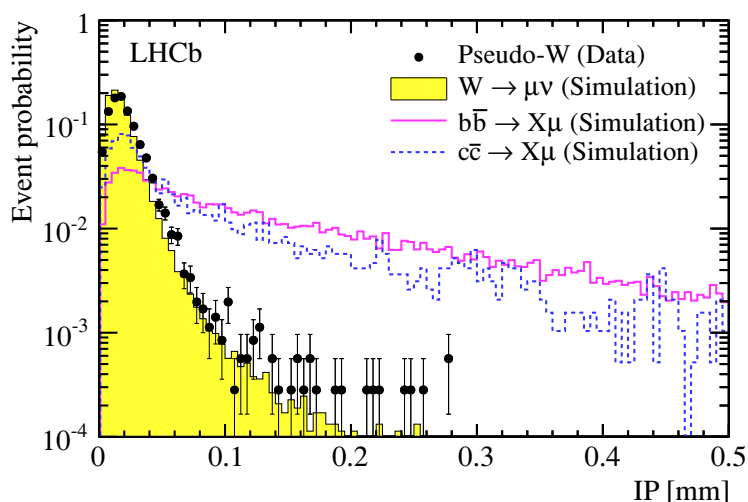


Figure 3. Muon IP distribution for pseudo- W events as points, W -MC as a yellow (shaded) histogram, and muons from simulated semi-leptonic decays of hadrons containing a b quark in the full open histogram or a c quark in the dashed open histogram. All distributions are normalised to unity.

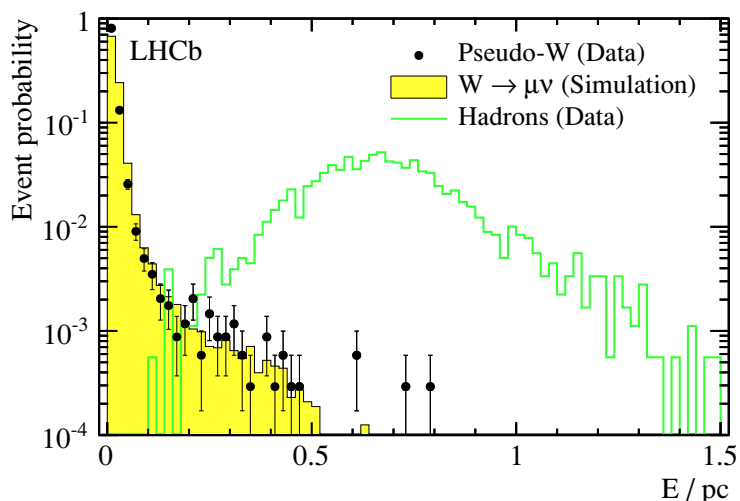


Figure 4. E/pc for pseudo- W events as points, W -MC as a yellow (shaded) histogram, and for hadrons from randomly triggered events in the open histogram. The energy E is the sum of the energies in the electromagnetic and hadronic calorimeter associated with the particle. All distributions are normalised to unity.

the particle, divided by the track momentum, p , for pseudo- W events, W -MC, and hadrons with $p_T > 20 \text{ GeV}/c$ in randomly triggered events. By requiring $E/pc < 0.04$ the punch-through contamination can be reduced to a negligible level. The disagreement between pseudo- W data and simulated W -MC in figure 4 is caused by the different underlying momentum distribution for muons from W and Z .

3.5 $W \rightarrow \mu\nu$ event yield

After the W selection requirements are imposed 14 660 W^+ and 11 618 W^- candidate events are observed. The $W \rightarrow \mu\nu$ signal yield has been determined by fitting the p_T^μ spectra of positive and negative muons in data, to template shapes for signal and backgrounds in five bins of η^μ . The fit is performed with the following sources for signal and background with the shapes and normalisations as described below.

1. The $W \rightarrow \mu\nu$ signal template is obtained using the W -MC. The normalisation is left free to vary in each bin of η^μ and for each charge.
2. The shape of the template of the largest background, $Z \rightarrow \mu\mu$, is taken from the Z -MC. The normalisation is fixed from data by counting the number of Z events, scaled by the ratio of events with one muon in the LHCb acceptance to events with both muons in the acceptance, as determined from Z -MC. The ratio is corrected for the different reconstruction and selection efficiencies for W and Z as derived from data. This gives an expectation of 2435 ± 101 background events ($(9.3 \pm 0.4)\%$ of the total sample) in good agreement with 2335 ± 25 events found from simulation.
3. The shape of the $W \rightarrow \tau\nu$ and $Z \rightarrow \tau\tau$ templates are taken from PYTHIA. The $Z \rightarrow \tau\tau$ template is scaled according to the observed number of Z events. These τ backgrounds constitute 2.7% of the total sample.
4. The heavy flavour template is obtained from data by requiring that the muon is not consistent with originating from the primary vertex ($IP > 80 \mu\text{m}$). The normalisation is determined from data applying all requirements except for the impact parameter and fitting the resulting IP distribution to the two templates shown in figure 3: the pseudo- W data to describe the signal, and the simulated heavy flavour events to describe the background. The heavy flavour contribution is estimated to be $(0.4 \pm 0.2)\%$ of the total sample.
5. The punch-through contribution from kaons and pions is largely suppressed by the requirement on E/pc . The E/pc distribution in figure 4 is fitted to pseudo- W data for the signal, and a Gaussian for the punch-through, in order to estimate the punch-through contribution. This is found to be negligible $(0.02 \pm 0.01)\%$ of the total sample, and also has a shape very similar to the decay-in-flight component. Hence, this component is not considered when determining the signal yield.
6. The decay-in-flight shape is found from data in a two-step procedure using all events selected throughout 2010 by any trigger requirement. First, tracks with a transverse momentum between 20 and 70 GeV/ c are taken to describe the p_T spectrum of hadrons; tracks that fired a muon trigger are excluded from the sample. Second, this spectrum is weighted according to the probability for a hadron to decay-in-flight. This probability is defined as the fraction of tracks identified as muons in randomly triggered events and is parametrised as a function of the momentum, p , by a function of the form

$$1 - e^{-\alpha/p}, \quad (3.1)$$

as would be expected for a particle whose mean lifetime in the laboratory frame scales with its boost. Consistent values for α are found in each pseudorapidity bin and are in agreement with a calculation of the decay probability based on the mean lifetimes for charged pions and kaons, and the distance to the electromagnetic calorimeter before which the hadron must have decayed. The average of the determinations in each pseudorapidity bin defines the central value for α . The relative normalisation of positively to negatively charged tracks in each bin of pseudorapidity is fixed to that observed in randomly triggered events, but the overall normalisation in each bin of pseudorapidity is left free.

The default fit has 15 free parameters: five parameters for the normalisation of W^+ in each of the pseudorapidity bins, five parameters for W^- , and five parameters for the contribution coming from the decay-in-flight. The normalisation of the other sources is fixed. The result of the fit is shown in figure 5. Integrated over both charges and p_T^μ it is found that $(44.3 \pm 1.2)\%$ of the total sample is due to W^+ , $(34.9 \pm 1.1)\%$ due to W^- , $(8.5 \pm 0.8)\%$ due to the decay-in-flight contribution and the remainder due to the other backgrounds. The χ^2/ndf of the fit is 1.002. The fit is repeated with the $Z \rightarrow \mu\mu$ and $W \rightarrow \mu\nu$ template corrected with RESBOS instead of NNLO, yielding $(43.6 \pm 1.2)\%$ for W^+ and $(34.4 \pm 1.1)\%$ for W^- with $\chi^2/\text{ndf} = 0.983$. The average of the two fits, which gives a purity $\rho^{W^+} = 0.788 \pm 0.021$ for W^+ and $\rho^{W^-} = 0.784 \pm 0.025$ for W^- , is taken for the final result; half of the difference is taken as the systematic uncertainty.

4 Cross-section measurement

4.1 Cross-section definition

Cross-sections are quoted in the kinematical range defined by the measurements. The cross-sections are measured in bins of η^μ for the W and in bins of y^Z in case of the Z . The cross-section in a given bin of y^Z (η^μ) is defined as

$$\sigma_{Z \rightarrow \mu\mu}(y^Z) = \frac{\rho^Z f_{\text{FSR}}^Z}{\mathcal{L} \mathcal{A}^Z} \sum_{\eta_i^\mu, \eta_j^\mu} \frac{N^Z(\eta_i^\mu, \eta_j^\mu)}{\varepsilon^Z(\eta_i^\mu, \eta_j^\mu)}, \quad \sigma_{W \rightarrow \mu\nu}(\eta^\mu) = \frac{\rho^W f_{\text{FSR}}^W N^W}{\mathcal{L} \mathcal{A}^W \varepsilon^W}, \quad (4.1)$$

where $N^Z(\eta_i^\mu, \eta_j^\mu)$ is the number of Z candidates in the respective y^Z bin with the two muons in the bins η_i^μ and η_j^μ being reconstructed with the efficiency $\varepsilon^Z(\eta_i^\mu, \eta_j^\mu)$. Similarly, N^W is the number of W candidates with the muon in the η^μ bin. The purity of the sample ($\rho^{Z(W)}$), the acceptance ($\mathcal{A}^{Z(W)}$), the correction factor for final state radiation (FSR) ($f_{\text{FSR}}^{Z(W)}$) and the efficiency (ε^W) are determined per bin; \mathcal{L} is the integrated luminosity. The total cross-section is obtained by summing the contributions of the five y^Z or η^μ bins.

4.2 Signal efficiencies

The data are corrected for efficiency losses due to track reconstruction, muon identification, and trigger requirements for both analyses. There is an additional selection efficiency in the W analysis due to the requirements on the number of additional muons, IP, E/pc , p_T^{cone} , E_T^{cone} , and on TT hits. All efficiencies are determined from data.

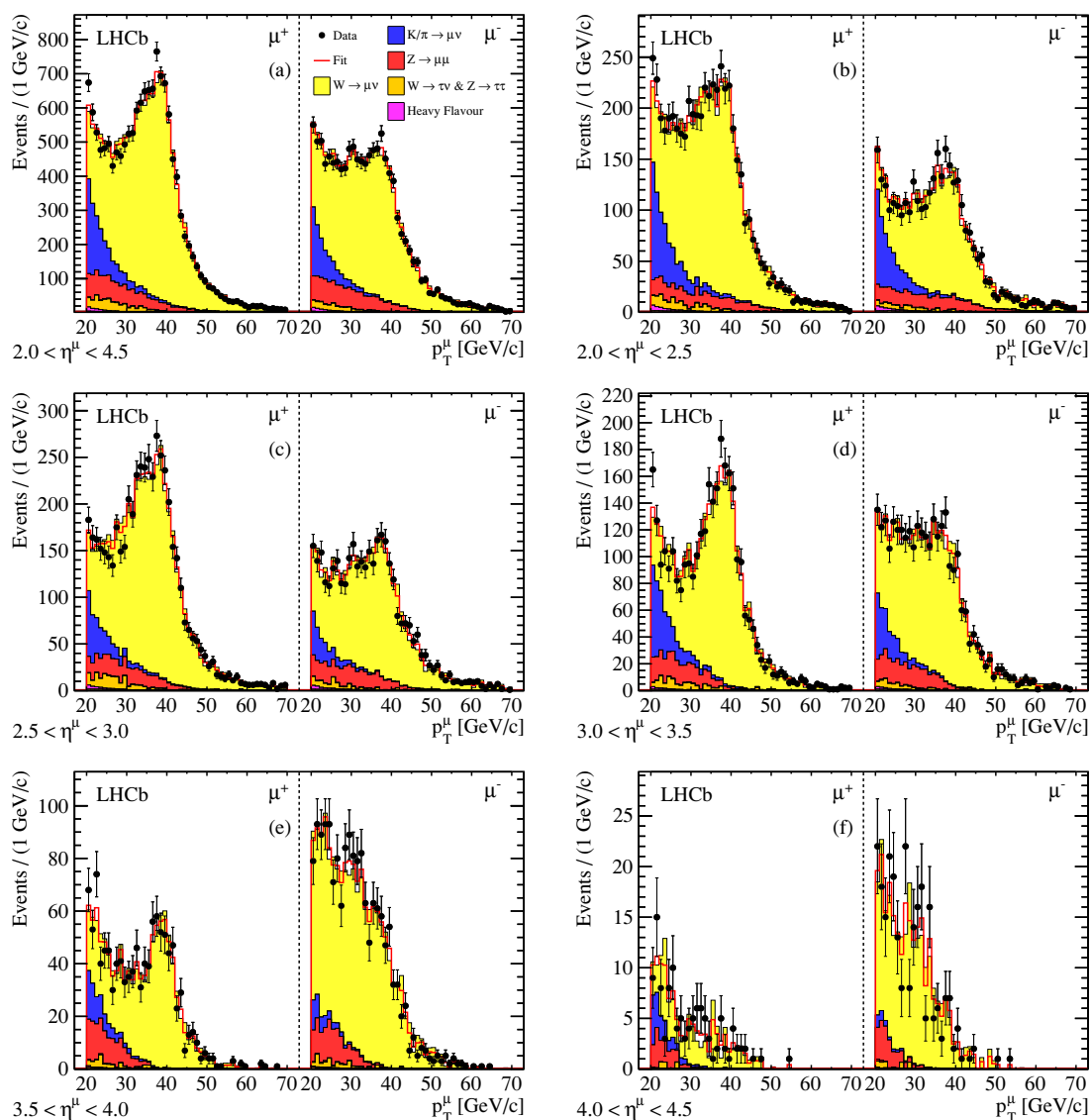


Figure 5. Distribution of muon p_T for positively (left panel) and negatively (right panel) charged muons in W candidate events, for the total fiducial cross-section (a). The plots (b) to (f) give the same information for the different η^μ bins. The data (points) are compared to the fitted contributions from W^- and W^+ (light shaded). The background contributions are, from top to bottom in the legend: decay-in-flight, $Z \rightarrow \mu\mu$, τ decays of W and Z , and heavy flavour decays.

The efficiencies for track reconstruction and muon identification are obtained using a tag-and-probe method in the Z sample. One of the muons in the Z sample (tag) satisfies all the track criteria. The other muon (probe) is selected with looser criteria that depend on the efficiency to be measured. The invariant mass of the dimuon candidates, reconstructed from the tag and the probe muons, must lie in the window of $20 \text{ GeV}/c^2$ around the nominal Z mass. The tracking efficiency, which accounts for track reconstruction and the track quality

requirements, is studied using well reconstructed tracks in the muon stations which are linked to hits in TT. The average track finding efficiency is about 90% in the Z sample and about 86% for the muon in W events. The tracking efficiency for W is lower due to the more restrictive cuts on the track quality. The muon identification efficiency is determined with tracks without the muon identification requirement for the probe muon. The average single muon efficiency is above 99%. Both the tracking and the muon identification efficiencies agree with simulation within errors.

The trigger efficiency contains two components, the first due to the efficiency of the single muon trigger and the other due to the global event cuts (GEC). The single muon trigger efficiency is determined using the $Z \rightarrow \mu\mu$ sample. One muon is required to fire the single muon trigger. The trigger response of the other muon then defines the trigger efficiency. The requirement on the occupancy of the events depends on the multiplicity of the primary interactions. It was checked with a sample which did not have the GEC applied, that no events are lost if there is only one primary vertex reconstructed. The GEC efficiency as a function of the number of primary vertices is determined by adding randomly triggered events to events with Z (W) candidates with one primary vertex; on average it amounts to 93%. The overall trigger efficiency is calculated for each event depending on the lepton pseudorapidity and the primary vertex multiplicity. It is found to be about 88% for the Z and 75% for the W sample.

The W selection requires that there are no other muons with $p_T^\mu > 2 \text{ GeV}/c$, $p_T^{\text{cone}} < 2 \text{ GeV}/c$, $E_T^{\text{cone}} < 2 \text{ GeV}$, $\text{IP} < 40 \mu\text{m}$, and $E/pc < 0.04$. The selection efficiency is determined from the fraction of pseudo- W events that pass these requirements. A similar method is used to evaluate the efficiency for the requirement of TT hits associated to the muon track of the W candidate. Simulation studies show that with the exception of the E/pc distribution, the pseudo- W data provide a consistent description of $W \rightarrow \mu\nu$ simulation, as shown in figures 2 and 3. However, the harder muon p_T spectrum in pseudo- W data leads to slightly lower values of E/pc than for muons produced in W decays. The simulation is used to determine this difference, which is only significant for η^μ between 2.0 and 2.5, where the efficiency for W events is estimated to be 2.1% lower than for pseudo- W data. The selection efficiency is about 67% for $2.5 < \eta^\mu < 4.0$ and drops to about 53% and 33% for the two bins at the edge of the acceptance with $2.0 < \eta^\mu < 2.5$ and $4.0 < \eta^\mu < 4.5$, respectively.

All the efficiencies have been checked for possible dependences on p_T^μ , the azimuthal angle of the muon, magnet polarity, and η^μ . Only the latter exhibits a significant dependence, which is taken into account. Since any charge bias of the efficiencies would directly influence the measurement of the lepton charge asymmetry, it was checked there is no significant charge dependence within the uncertainties of the efficiencies. The efficiency corrections are applied as a function of the pseudorapidity of the muons except the GEC.

The efficiencies are uncorrelated between pseudorapidity bins but correlated for W^+ , W^- and Z . These correlations are taken into account for the measurement of the lepton charge asymmetry and the cross-section ratios.

4.3 Acceptance

The selection criteria for the W and Z define the fiducial region of the measurement. Simulated events are used to determine the acceptance \mathcal{A} , defined as $\mathcal{A} = N_{\text{rec}}/N_{\text{gen}}$. Here, N_{rec} is the number of reconstructed events satisfying the cuts on the pseudorapidity and the minimal momenta of the reconstructed muons, as well as on the dimuon mass in the case of the Z analysis. Similarly, N_{gen} is the number of generated events with the cuts applied on the generated muons. The acceptance is estimated with W -MC and Z -MC. It is found to be consistent with unity for the Z and above 0.99 for the W analysis. For the latter, the acceptance corrects for the small loss of events with $p_{\text{T}}^{\mu} > 70 \text{ GeV}/c$.

4.4 Luminosity

The absolute luminosity scale was measured at specific periods during the data taking, using both Van der Meer scans [28] where colliding beams are moved transversely across each other to determine the beam profile, and a beam-gas imaging method [29, 30]. For the latter, reconstructed beam-gas interaction vertices near the beam crossing point determine the beam profile. Both methods give similar results and are estimated to have a precision of order 3.5%. The knowledge of the absolute luminosity scale is used to calibrate the number of tracks in the VELO, which is found to be stable throughout the data-taking period and can therefore be used to monitor the instantaneous luminosity of the entire data sample. The dataset for this analysis corresponds to an integrated luminosity of $37.1 \pm 1.3 \text{ pb}^{-1}$.

4.5 Corrections to the data

The measured cross-sections are corrected to Born level in quantum electrodynamics (QED) in order to provide a consistent comparison with NLO and NNLO QCD predictions, which do not include the effects of FSR. Corrections have been estimated using PHOTOS [31] interfaced to PYTHIA. The PYTHIA p_{T} spectrum of the electroweak boson has been reweighted to the NNLO spectrum as determined with DYNLO [23]. The correction is taken as the number of events within the fiducial cuts of the measurements after FSR divided by the number of events generated within the fiducial cuts.

PYTHIA simulation is used to study bin-to-bin migrations for η^{μ} and y^Z . No significant net migration is observed and no correction is applied.

4.6 Systematic uncertainties

Aside from the uncertainty on the luminosity measurement, the main sources of experimental uncertainties come from the efficiency determinations and the background estimate in the W analysis. The following sources have been considered:

1. The relative uncertainties of the tracking, muon identification, trigger and GEC efficiencies are added in quadrature. They lead to a systematic uncertainty for the total cross-sections of 4.3% (2.2%, 2.0%) for the Z (W^+ , W^-).
2. The statistical uncertainty on the efficiency of the additional selection cuts for the W analysis translates into a 1.8% (1.7%) systematic uncertainty on the total W^+ (W^-) cross-section.

Source	$\Delta\sigma_{Z\rightarrow\mu\mu}$ (%)	$\Delta\sigma_{W^+\rightarrow\mu^+\nu}$ (%)	$\Delta\sigma_{W^-\rightarrow\mu^-\bar{\nu}}$ (%)
Signal purity	± 0.1	± 1.2	± 0.9
Template shape (fit)	—	± 0.9	± 1.0
Efficiency (trigger, tracking, muon id)	± 4.3	± 2.2	± 2.0
Additional selection	—	± 1.8	± 1.7
FSR correction	± 0.02	± 0.01	± 0.02
Total	± 4.3	± 3.2	± 2.9
Luminosity	± 3.5	± 3.5	± 3.5

Table 1. Contributions to the systematic uncertainty for the total Z and W cross-sections. The different contributions are discussed in section 4.6

3. The uncertainty of the background contribution for the Z analysis is small; the uncertainty in the determination of the sample purity leads to a 0.1% uncertainty on the total cross-section.
4. Both the shape and normalisations of the templates used in the W fit are considered as an additional source of uncertainty. To determine this systematic uncertainty each of the following sources is varied in turn, the data are refitted to determine the fraction of W^+ and W^- events, and the deviations from the original signal yield are combined in quadrature. The following variations are made:
 - the difference of the two fits using different W and Z templates (see section 3.5) leads to a variation on the W fractions of 0.8%;
 - the normalisation of the Z component was changed by the statistical uncertainty with which it was determined, leading to a variation in the W fractions of 0.3%;
 - the normalisation of the $W \rightarrow \tau\nu$ template was changed by the statistical uncertainty with which it was determined, leading to a negligible change in the W fractions, since this template shape is very similar to the decay-in-flight template which is allowed to vary in the fit;
 - the heavy flavour template has also been changed by the statistical uncertainty with which it was determined leading to a negligible change in the W fractions;
 - instead of leaving the relative normalisation of the decays-in-flight template between pseudorapidity bins to be free in the fit, this is fixed to the values observed in randomly triggered events, and the full fit performed with a single free parameter for the background; the W fractions change by 0.2%;
 - the shape of the decay-in-flight template has been changed using different values for α (see eq. (3.1)) to describe the decay probability, corresponding to different regions in which the hadron must have decayed;³ no difference in the W fractions is observed.

³Three different decay regions have been considered: from the interaction point, from the VELO and from the TT stations up to the electromagnetic calorimeter.

5. The uncertainty on the FSR correction is evaluated for each bin as the maximum of the statistical uncertainty of the correction factor and the difference between the weighted and unweighted FSR correction factor.

The sources of systematic uncertainties are summarised in table 1, together with the size of the resultant uncertainty on the W and Z total cross-sections. The total systematic uncertainty is the sum of all contributions added in quadrature.

5 Results

The inclusive cross-sections for $Z \rightarrow \mu\mu$ and $W \rightarrow \mu\nu$ production for muons with $p_{\text{T}}^{\mu} > 20 \text{ GeV}/c$ in the pseudorapidity region $2.0 < \eta^{\mu} < 4.5$ and, in the case of Z , the invariant mass range $60 < M_{\mu\mu} < 120 \text{ GeV}/c^2$ are measured to be

$$\begin{aligned}\sigma_{Z \rightarrow \mu\mu} &= 76.7 \pm 1.7 \pm 3.3 \pm 2.7 \text{ pb} \\ \sigma_{W^+ \rightarrow \mu^+\nu} &= 831 \pm 9 \pm 27 \pm 29 \text{ pb} \\ \sigma_{W^- \rightarrow \mu^-\bar{\nu}} &= 656 \pm 8 \pm 19 \pm 23 \text{ pb},\end{aligned}$$

where the first uncertainty is statistical, the second systematic and the third is due to the luminosity. All the measurements are dominated by the luminosity and the systematic uncertainty. The latter is dominated by the limited number of events for the background templates and in the determination of the efficiencies.

The ratios $R_W = \sigma_{W^+ \rightarrow \mu^+\nu} / \sigma_{W^- \rightarrow \mu^-\bar{\nu}}$ and $R_{WZ} = (\sigma_{W^+ \rightarrow \mu^+\nu} + \sigma_{W^- \rightarrow \mu^-\bar{\nu}}) / \sigma_{Z \rightarrow \mu\mu}$ are measured to be

$$\begin{aligned}R_W &= 1.27 \pm 0.02 \pm 0.01 \\ R_{WZ} &= 19.4 \pm 0.5 \pm 0.9.\end{aligned}$$

Here, the uncertainty from the luminosity completely cancels. The systematic uncertainty on the trigger, muon identification, tracking and selection efficiencies, as well as the uncertainty on the purity are assumed to be fully correlated between W^+ and W^- . No correlation is assumed between the η^{μ} bins, except for the purity. The uncertainty on the Z cross-section from the reconstruction efficiency is correlated between boson rapidity bins. The correlation of the uncertainty on the efficiencies between W and Z are estimated with MC simulation to be 90%. The full correlation matrix is given in the appendix (table 2). The ratio of the W to Z cross-section is measured, for each charge separately, to be

$$\begin{aligned}\sigma_{W^+ \rightarrow \mu^+\nu} / \sigma_{Z \rightarrow \mu\mu} &= 10.8 \pm 0.3 \pm 0.5 \\ \sigma_{W^- \rightarrow \mu^-\bar{\nu}} / \sigma_{Z \rightarrow \mu\mu} &= 8.5 \pm 0.2 \pm 0.4.\end{aligned}$$

A summary of the measurements of the inclusive cross-sections $\sigma_{W^+ \rightarrow \mu^+\nu}$, $\sigma_{W^- \rightarrow \mu^-\bar{\nu}}$ and $\sigma_{Z \rightarrow \mu\mu}$, and the ratios is shown in figure 6. The measurements are shown as a band which represents the total and statistical uncertainties.

The results are compared to theoretical predictions calculated at NNLO with the program DYNLO [23] for the NNLO PDF sets of MSTW08 [32], ABKM09 [33], JR09 [34], HERA15 [12] and NNPDF21 [35] and at NLO for the NLO PDF set CTEQ6m [16].⁴ The

⁴DYNLO sets α_s to the value of α_s at the mass of the Z boson as given by the different PDF sets.

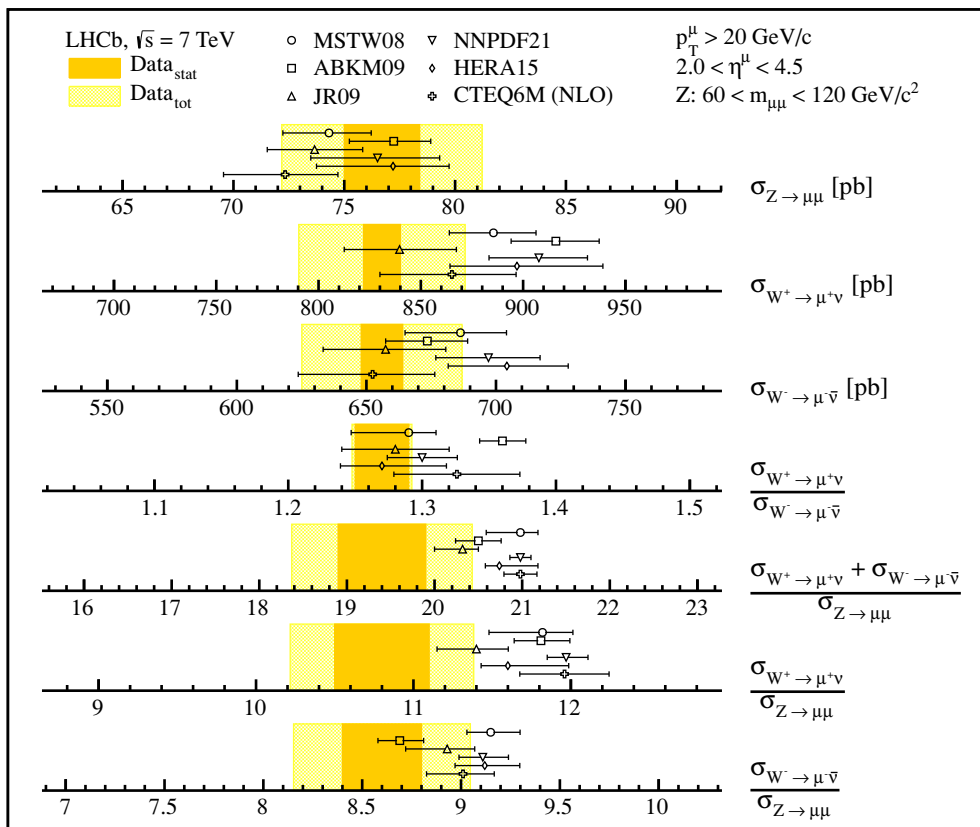


Figure 6. Measurements of the Z , W^+ and W^- cross-section and ratios, data are shown as bands which the statistical (dark shaded/orange) and total (light hatched/yellow) errors. The measurements are compared to NNLO and NLO predictions with different PDF sets for the proton, shown as points with error bars. The PDF uncertainty, evaluated at the 68% confidence level, and the theoretical uncertainties are added in quadrature to obtain the uncertainties of the predictions.

scale uncertainties are estimated by varying the renormalisation and factorisation scales by factors of two around the nominal value, which is set to the boson mass. The uncertainties for each set correspond to the PDF uncertainties at 68% and the scale uncertainties added in quadrature.⁵

While the W^- and Z cross-sections are well described by all predictions, the W^+ cross-section is slightly overestimated by the ABKM09 and NNPDF21 PDF sets. The ratio of the W^- to Z cross-sections agrees reasonably well with the predictions, but the W^+ to the Z ratio is overestimated by most of the predictions. The systematic uncertainties for the R_W almost cancel and also the theoretical uncertainties are much reduced. The R_W measurement tests the Standard Model predictions with a precision of 1.7% which is comparable to the uncertainty of the theoretical prediction. The ABKM09 prediction overestimates this ratio while all the other predictions agree with the measurement. Differential distributions are measured in five bins in y^Z for the Z and of η^μ for the W . Figure 7 shows the differential cross-section as a function of the rapidity of the Z boson together with

⁵The uncertainties for the PDF set from CTEQ6m which is given at 90% CL are divided by 1.645.

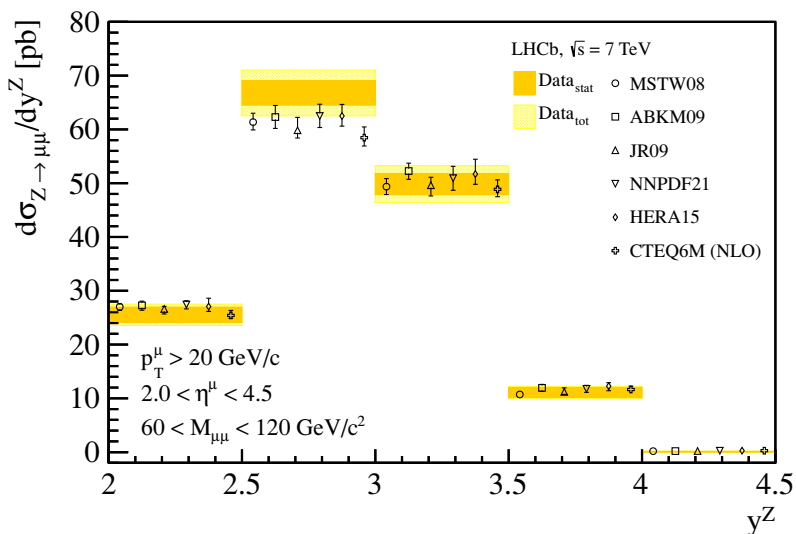


Figure 7. Differential cross-section for $Z \rightarrow \mu\mu$ as a function of y^Z . The dark shaded (orange) bands correspond to the statistical uncertainties, the light hatched (yellow) band to the statistical and systematic uncertainties added in quadrature. Superimposed are NNLO (NLO) predictions with different parametrisations for the PDF as points with error bars; they are displaced horizontally for presentation.

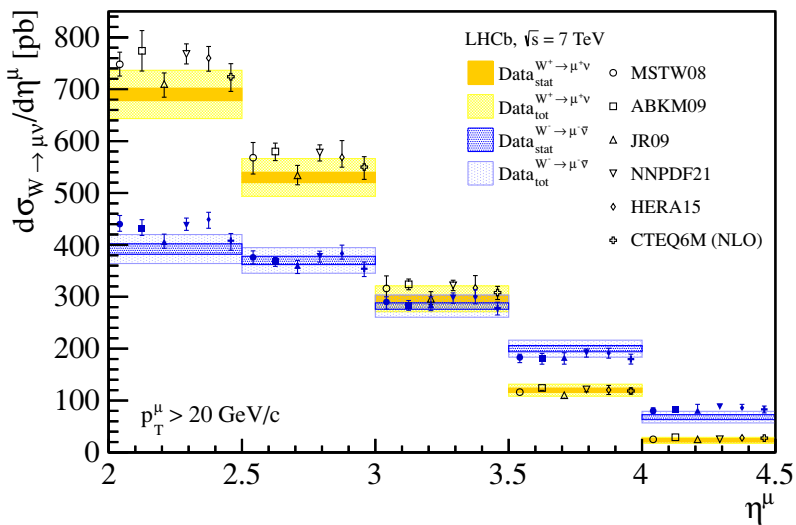


Figure 8. Differential W cross-section in bins of muon pseudorapidity. The dark shaded (orange) bands correspond to the statistical uncertainties, the light hatched (yellow) band to the statistical and systematic uncertainties added in quadrature. Superimposed are NNLO (NLO) predictions as described in figure 7.

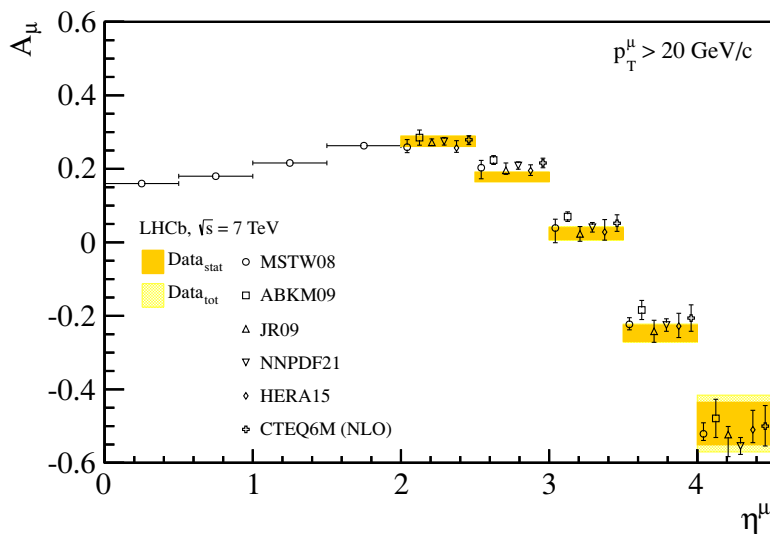


Figure 9. Lepton charge asymmetry $A_\mu = (\sigma_{W^+ \rightarrow \mu^+ \nu} - \sigma_{W^- \rightarrow \mu^- \bar{\nu}}) / (\sigma_{W^+ \rightarrow \mu^+ \nu} + \sigma_{W^- \rightarrow \mu^- \bar{\nu}})$ in bins of muon pseudorapidity. The dark shaded (orange) bands correspond to the statistical uncertainties, the light hatched (yellow) band to the statistical and systematic uncertainties added in quadrature. Superimposed are NNLO (NLO) predictions as described in figure 7. The MSTW08 values for $\eta^\mu < 2$ represent the central value of the prediction.

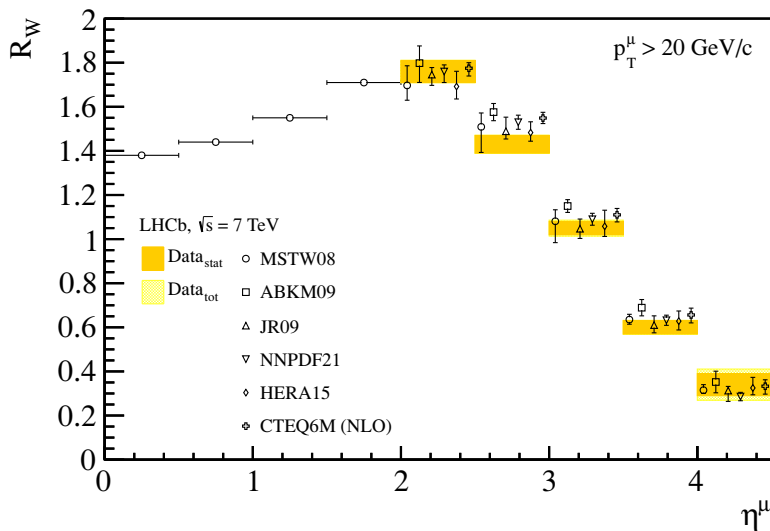


Figure 10. $R_W = \sigma_{W^+ \rightarrow \mu^+ \nu} / \sigma_{W^- \rightarrow \mu^- \bar{\nu}}$ in bins of muon pseudorapidity. The dark shaded (orange) bands correspond to the statistical uncertainties, the light hatched (yellow) band to the statistical and systematic uncertainties added in quadrature. Superimposed are NNLO (NLO) predictions with different parametrisations as described in figure 7. The MSTW08 values for $\eta^\mu < 2$ represent the central value of the prediction.

NNLO (NLO) predictions with different parametrisation for the PDFs of the proton. The predictions agree with the measurements within uncertainties though all the predictions are lower than the measured cross-section for $2.5 < \eta^\mu < 3.0$. The differential cross-sections are listed in table 3 in the appendix.

The differential distribution of the W^+ and W^- cross-section, the lepton charge asymmetry A_μ and the ratio R_W as a function of the muon pseudorapidity are shown in figures 8, 9 and 10 and listed in tables 4 to 6 as a function of p_T^μ . The measurement of the charge asymmetry and the W ratio provides important additional information on the PDFs particularly on the valence quark distributions [11].

Since the inclusive cross-section for W^+ is larger than for W^- , due to the excess of u over d quarks in the proton, the overall asymmetry is positive. The asymmetry and the W cross-sections strongly vary as a function of the pseudorapidity of the charged lepton, and A_μ even changes sign, owing to differing helicity dependence of the lepton couplings to the boson. This behaviour is reflected in the differential W cross-sections, where at large muon pseudorapidities the W^- cross-section is higher than the W^+ cross-section, as a consequence of the $V - A$ structure of the W to lepton coupling. The cross-section and the asymmetry measurements are compared to the NNLO (NLO) predictions with different parameterisation for the PDFs. The ABKM09 prediction overestimates the measured asymmetry in three of the five bins. The other predictions describe the measurement within uncertainties.

The asymmetry is also measured for two higher p_T^μ thresholds for the muons, at 25 and 30 GeV/ c . The result is shown in figure 11 and listed in table 5. The NNLO prediction with MSTW08 parametrisation for the PDF also describes the measured asymmetry with the higher cuts on the transverse momentum of the muon.

6 Conclusions

Measurements of inclusive W and Z boson production in pp collisions at $\sqrt{s} = 7$ TeV with final states containing muons have been performed using 37 pb^{-1} of data collected with the LHCb detector. The inclusive cross-sections have been measured separately for W^+ and W^- production as well as the ratios $\sigma_{W^+ \rightarrow \mu^+ \nu} / \sigma_{W^- \rightarrow \mu^- \bar{\nu}}$ and $(\sigma_{W^+ \rightarrow \mu^+ \nu} + \sigma_{W^- \rightarrow \mu^- \bar{\nu}}) / \sigma_{Z \rightarrow \mu \mu}$ and the lepton charge asymmetry $(\sigma_{W^+ \rightarrow \mu^+ \nu} - \sigma_{W^- \rightarrow \mu^- \bar{\nu}}) / (\sigma_{W^+ \rightarrow \mu^+ \nu} + \sigma_{W^- \rightarrow \mu^- \bar{\nu}})$. The results have been compared to five next-to-next-to-leading order QCD predictions with different sets for the parton density functions of the proton and to one calculation at next-to-leading order. There is general agreement with the predictions, though some of the PDF sets overestimate the ratios of the cross-sections. The ratio $\sigma_{W^+ \rightarrow \mu^+ \nu} / \sigma_{W^- \rightarrow \mu^- \bar{\nu}} = 1.27 \pm 0.02 \pm 0.01$ is measured precisely and allows the Standard Model prediction to be tested with an accuracy of about 1.7%, comparable to the uncertainty on the theory prediction. These represent the first measurements of the W and Z production cross-sections and ratios in the forward region at the LHC, and will provide valuable input to the knowledge of the parton density functions of the proton. The uncertainty on the cross-section measurements is dominated by systematic uncertainties. Since most of these are statistical in nature, the accuracy on the measurement with further data is expected to significantly improve.

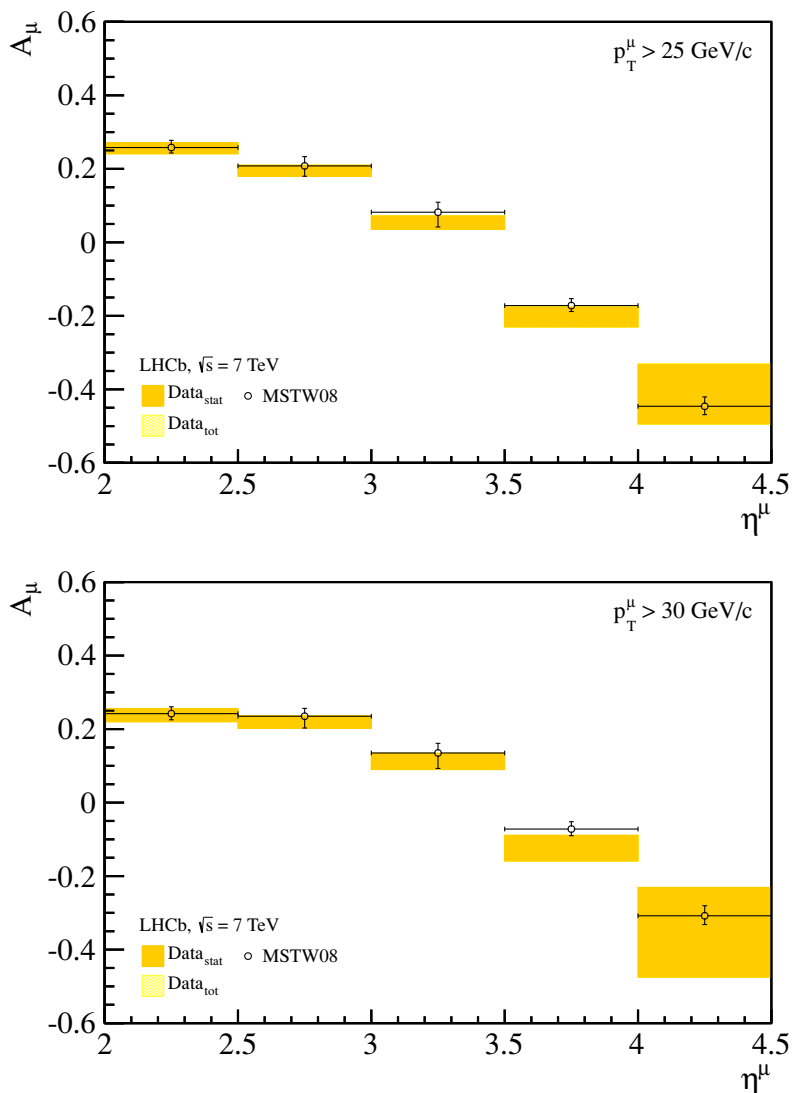


Figure 11. Lepton charge asymmetry $A_\mu = (\sigma_{W^+ \rightarrow \mu^+ \nu} - \sigma_{W^- \rightarrow \mu^- \bar{\nu}}) / (\sigma_{W^+ \rightarrow \mu^+ \nu} + \sigma_{W^- \rightarrow \mu^- \bar{\nu}})$ for muons with $p_T^\mu > 25$ (top) and $30 \text{ GeV}/c$ (bottom), respectively in bins of muon pseudorapidity. The dark shaded (orange) bands correspond to the statistical uncertainties, the light hatched (yellow) band to the statistical and systematic uncertainties added in quadrature. The statistical uncertainty is undistinguishable from the total uncertainty. Superimposed are the NNLO predictions with the MSTW08 parametrisation for the PDF.

Acknowledgments

We express our gratitude to our colleagues in the CERN accelerator departments for the excellent performance of the LHC. We thank the technical and administrative staff at CERN and at the LHCb institutes, and acknowledge support from the National Agencies: CAPES, CNPq, FAPERJ and FINEP (Brazil); CERN; NSFC (China); CNRS/IN2P3 (France); BMBF, DFG, HGF and MPG (Germany); SFI (Ireland); INFN (Italy); FOM

and NWO (The Netherlands); SCSR (Poland); ANCS (Romania); MinES of Russia and Rosatom (Russia); MICINN, XuntaGal and GENCAT (Spain); SNSF and SER (Switzerland); NAS Ukraine (Ukraine); STFC (United Kingdom); NSF (U.S.A.). We also acknowledge the support received from the ERC under FP7 and the Region Auvergne.

A Tables of results

	$2 < \eta^\mu (y^Z) < 2.5$			$2.5 < \eta^\mu (y^Z) < 3$			$3 < \eta^\mu (y^Z) < 3.5$			$3.5 < \eta^\mu (y^Z) < 4$			$4 < \eta^\mu (y^Z) < 4.5$			
W^+	1															$2 < \eta^\mu (y^Z) < 2.5$
W^-	0.87	1														
Z	0.36	0.34	1													
W^+	0.02	0.02	0.35	1												$2.5 < \eta^\mu (y^Z) < 3$
W^-	0.02	0.02	0.35	0.90	1											
Z	0.47	0.44	0.45	0.45	0.45	1										
W^+	0.02	0.03	0.24	0.02	0.02	0.31	1									$3 < \eta^\mu (y^Z) < 3.5$
W^-	0.02	0.02	0.29	0.02	0.02	0.37	0.89	1								
Z	0.46	0.43	0.44	0.45	0.44	0.58	0.31	0.37	1							
W^+	0.04	0.05	0.35	0.04	0.04	0.45	0.05	0.04	0.44	1						$3.5 < \eta^\mu (y^Z) < 4$
W^-	0.02	0.02	0.40	0.02	0.01	0.52	0.02	0.02	0.51	0.80	1					
Z	0.32	0.29	0.30	0.30	0.30	0.39	0.21	0.25	0.39	0.30	0.35	1				
W^+	0.07	0.09	0.19	0.07	0.07	0.24	0.09	0.07	0.24	0.15	0.06	0.16	1			$4 < \eta^\mu (y^Z) < 4.5$
W^-	0.01	0.01	0.28	0.01	0.01	0.37	0.01	0.01	0.36	0.02	0.01	0.24	0.57	1		
Z	0.03	0.03	0.03	0.03	0.03	0.04	0.02	0.03	0.04	0.03	0.04	0.03	0.02	0.03	1	
	W^+	W^-	Z	W^+	W^-	Z										

Table 2. Correlation coefficients between W^+ , W^- and Z in the five bins considered. The luminosity uncertainty is not included.

y^Z	$d\sigma_{Z \rightarrow \mu\mu}/dy^Z$ [pb]				f_{FSR}^Z
2.0 – 2.5	25.5	± 1.4	± 1.0	± 0.9	1.020 ± 0.001
2.5 – 3.0	66.8	± 2.3	± 2.7	± 2.3	1.018 ± 0.001
3.0 – 3.5	49.8	± 2.0	± 2.2	± 1.7	1.018 ± 0.001
3.5 – 4.0	11.1	± 0.9	± 0.6	± 0.4	1.024 ± 0.001
4.0 – 4.5	0.074	± 0.074	± 0.004	± 0.002	1.027 ± 0.027

Table 3. Differential $Z \rightarrow \mu\mu$ cross-section, $d\sigma_{Z \rightarrow \mu\mu}/dy^Z$, in bins of boson rapidity. The first cross-section uncertainty is statistical, the second systematic, and the third due to the uncertainty on the luminosity determination. The correction factor f_{FSR}^Z which is used to correct for FSR is listed separately.

	η^μ	$d\sigma_{W \rightarrow \mu\nu}/\eta^\mu$ [pb]				f_{FSR}^W
W^+	2.0 – 2.5	691	± 12	± 37	± 24	1.0146 ± 0.0004
	2.5 – 3.0	530	± 9	± 30	± 19	1.0086 ± 0.0002
	3.0 – 3.5	296	± 7	± 23	± 10	1.0107 ± 0.0006
	3.5 – 4.0	121	± 5	± 19	± 4	1.0097 ± 0.0005
	4.0 – 4.5	23.1	± 3.2	± 4.9	± 0.8	1.0009 ± 0.0009
W^-	2.0 – 2.5	393	± 9	± 22	± 13	1.0147 ± 0.0008
	2.5 – 3.0	370	± 8	± 20	± 13	1.0163 ± 0.0004
	3.0 – 3.5	282	± 7	± 18	± 10	1.0147 ± 0.0004
	3.5 – 4.0	200	± 6	± 14	± 7	1.0173 ± 0.0008
	4.0 – 4.5	68	± 5	± 10	± 2	1.0194 ± 0.0009

Table 4. Differential $W \rightarrow \mu\nu$ cross-section, $d\sigma_{W \rightarrow \mu\nu}/\eta^\mu$, in bins of lepton pseudorapidity. The first cross-section uncertainty is statistical, the second systematic, and the third due to the uncertainty on the luminosity determination. The correction factor f_{FSR}^W which is used to correct for FSR is listed separately.

η^μ	$A_\mu (p_T^\mu > 20 \text{ GeV}/c)$			$A_\mu (p_T^\mu > 25 \text{ GeV}/c)$			$A_\mu (p_T^\mu > 30 \text{ GeV}/c)$		
2.0–2.5	0.275	± 0.014	± 0.003	0.256	± 0.015	± 0.002	0.238	± 0.018	± 0.002
2.5–3.0	0.178	± 0.013	± 0.002	0.195	± 0.015	± 0.001	0.219	± 0.017	± 0.001
3.0–3.5	0.024	± 0.016	± 0.009	0.054	± 0.018	± 0.003	0.112	± 0.022	± 0.002
3.5–4.0	-0.247	± 0.022	± 0.011	-0.203	± 0.027	± 0.005	-0.124	± 0.035	± 0.003
4.0–4.5	-0.493	± 0.058	± 0.051	-0.413	± 0.081	± 0.016	-0.353	± 0.122	± 0.008

Table 5. Lepton charge asymmetry, A_μ , in bins of muon pseudorapidity for a p_T^μ threshold at 20, 25 and 30 GeV/c. The first uncertainty is statistical and the second systematic. The effect of FSR is at the level of 10^{-4} and is not listed.

η^μ	R_W		
2.0 – 2.5	1.76	± 0.05	± 0.01
2.5 – 3.0	1.43	± 0.04	± 0.01
3.0 – 3.5	1.05	± 0.03	± 0.02
3.5 – 4.0	0.60	± 0.03	± 0.01
4.0 – 4.5	0.34	± 0.05	± 0.05

Table 6. W cross-section ratio, $R_W = \sigma_{W^+ \rightarrow \mu^+ \nu} / \sigma_{W^- \rightarrow \mu^- \bar{\nu}}$, in bins of muon pseudorapidity. The first error is statistical and the second systematic. The effect of FSR is at the level of 10^{-4} and is not listed.

Open Access. This article is distributed under the terms of the Creative Commons Attribution License which permits any use, distribution and reproduction in any medium, provided the original author(s) and source are credited.

References

- [1] ATLAS collaboration, G. Aad et al., *Measurement of the $W \rightarrow l\nu$ and $Z/\gamma^* \rightarrow ll$ production cross sections in proton-proton collisions at $\sqrt{s} = 7$ TeV with the ATLAS detector*, *JHEP* **12** (2010) 060 [[arXiv:1010.2130](#)] [[INSPIRE](#)].
- [2] ATLAS collaboration, G. Aad et al., *Measurement of the muon charge asymmetry from W bosons produced in pp collisions at $\sqrt{s} = 7$ TeV with the ATLAS detector*, *Phys. Lett.* **B 701** (2011) 31 [[arXiv:1103.2929](#)] [[INSPIRE](#)].
- [3] CMS collaboration, S. Chatrchyan et al., *Measurement of the inclusive W and Z production cross sections in pp collisions at $\sqrt{s} = 7$ TeV*, *JHEP* **10** (2011) 132 [[arXiv:1107.4789](#)] [[INSPIRE](#)].
- [4] CMS collaboration, S. Chatrchyan et al., *Measurement of the lepton charge asymmetry in inclusive W production in pp collisions at $\sqrt{s} = 7$ TeV*, *JHEP* **04** (2011) 050 [[arXiv:1103.3470](#)] [[INSPIRE](#)].
- [5] UA1 collaboration, C. Albajar et al., *Intermediate vector boson cross-sections at the CERN super proton synchrotron collider and the number of neutrino types*, *Phys. Lett.* **B 198** (1987) 271 [[INSPIRE](#)].
- [6] UA2 collaboration, J. Alitti et al., *A measurement of the W and Z production cross-sections and a determination of γ (W) at the CERN $\bar{p}p$ collider*, *Phys. Lett.* **B 276** (1992) 365 [[INSPIRE](#)].
- [7] CDF collaboration, F. Abe et al., *Measurement of $\sigma \cdot B(W \rightarrow e\nu)$ and $\sigma \cdot B(Z^0 \rightarrow e^+e^-)$ in $p\bar{p}$ collisions at $\sqrt{s} = 1.8$ TeV*, *Phys. Rev. Lett.* **76** (1996) 3070 [[hep-ex/9509010](#)] [[INSPIRE](#)].
- [8] CDF collaboration, F. Abe et al., *Measurement of Z^0 and Drell-Yan production cross section using dimuons in $p\bar{p}$ collisions at $\sqrt{s} = 1.8$ TeV*, *Phys. Rev.* **D 59** (1999) 052002 [[INSPIRE](#)].
- [9] CDF collaboration, A. Abulencia et al., *Measurements of inclusive W and Z cross sections in $p\bar{p}$ collisions at $\sqrt{s} = 1.96$ TeV*, *J. Phys.* **G 34** (2007) 2457 [[hep-ex/0508029](#)] [[INSPIRE](#)].

- [10] D0 collaboration, B. Abbott et al., *Extraction of the width of the W boson from measurements of $\sigma(p\bar{p} \rightarrow W + X) \times B(W \rightarrow e\nu)$ and $\sigma(p\bar{p} \rightarrow Z + X) \times B(Z \rightarrow ee)$ and their ratio*, *Phys. Rev. D* **61** (2000) 072001 [[hep-ex/9906025](#)] [[INSPIRE](#)].
- [11] E.L. Berger, F. Halzen, C. Kim and S. Willenbrock, *Weak boson production at Tevatron energies*, *Phys. Rev. D* **40** (1989) 83 [*Erratum ibid.* **D 40** (1989) 3789] [[INSPIRE](#)].
- [12] H1 AND ZEUS collaboration, F. Aaron et al., *Combined measurement and QCD analysis of the inclusive $e^{+-}p$ scattering cross sections at HERA*, *JHEP* **01** (2010) 109 [[arXiv:0911.0884](#)] [[INSPIRE](#)].
- [13] LHCb collaboration, J. Alves, A. Augusto et al., *The LHCb detector at the LHC*, 2008 *JINST* **3** S08005 [[INSPIRE](#)].
- [14] T. Sjöstrand, S. Mrenna and P.Z. Skands, *PYTHIA 6.4 physics and manual*, *JHEP* **05** (2006) 026 [[hep-ph/0603175](#)] [[INSPIRE](#)].
- [15] LHCb collaboration, M. Clemencic et al., *The LHCb simulation application, Gauss: Design, evolution and experience*, *J. Phys. Conf. Ser.* **331** (2011) 032023 [[INSPIRE](#)].
- [16] P.M. Nadolsky, H.-L. Lai, Q.-H. Cao, J. Huston, J. Pumplin, et al., *Implications of CTEQ global analysis for collider observables*, *Phys. Rev. D* **78** (2008) 013004 [[arXiv:0802.0007](#)] [[INSPIRE](#)].
- [17] M. Bengtsson and T. Sjöstrand, *Parton showers in lepton production events*, *Z. Phys. C* **37** (1988) 465 [[INSPIRE](#)].
- [18] B. Andersson, G. Gustafson, G. Ingelman and T. Sjöstrand, *Parton fragmentation and string dynamics*, *Phys. Rept.* **97** (1983) 31 [[INSPIRE](#)].
- [19] GEANT4 collaboration, S. Agostinelli et al., *GEANT4: a simulation toolkit*, *Nucl. Instrum. Meth. A* **506** (2003) 250 [[INSPIRE](#)].
- [20] P. Nason, *A new method for combining NLO QCD with shower Monte Carlo algorithms*, *JHEP* **11** (2004) 040 [[hep-ph/0409146](#)] [[INSPIRE](#)].
- [21] S. Frixione, P. Nason and C. Oleari, *Matching NLO QCD computations with parton shower simulations: the POWHEG method*, *JHEP* **11** (2007) 070 [[arXiv:0709.2092](#)] [[INSPIRE](#)].
- [22] S. Alioli, P. Nason, C. Oleari and E. Re, *A general framework for implementing NLO calculations in shower Monte Carlo programs: the POWHEG BOX*, *JHEP* **06** (2010) 043 [[arXiv:1002.2581](#)] [[INSPIRE](#)].
- [23] S. Catani, L. Cieri, G. Ferrera, D. de Florian and M. Grazzini, *Vector boson production at hadron colliders: a fully exclusive QCD calculation at NNLO*, *Phys. Rev. Lett.* **103** (2009) 082001 [[arXiv:0903.2120](#)] [[INSPIRE](#)].
- [24] G. Ladinsky and C. Yuan, *The nonperturbative regime in QCD resummation for gauge boson production at hadron colliders*, *Phys. Rev. D* **50** (1994) 4239 [[hep-ph/9311341](#)] [[INSPIRE](#)].
- [25] C. Balázs and C. Yuan, *Soft gluon effects on lepton pairs at hadron colliders*, *Phys. Rev. D* **56** (1997) 5558 [[hep-ph/9704258](#)] [[INSPIRE](#)].
- [26] F. Landry, R. Brock, P.M. Nadolsky and C. Yuan, *Tevatron Run-1 Z boson data and Collins-Soper-Sterman resummation formalism*, *Phys. Rev. D* **67** (2003) 073016 [[hep-ph/0212159](#)] [[INSPIRE](#)].
- [27] T. Skwarnicki, *A study of the radiative cascade transitions between the Υ' and Υ resonances*, Ph.D. thesis, Institute of Nuclear Physics, Krakow Poland (1986) [[DESY-F31-86-02](#)].

- [28] S. van der Meer, *Calibration of the effective beam height in the ISR*, **ISR-PO/68-31** (1968).
- [29] M. Ferro-Luzzi, *Proposal for an absolute luminosity determination in colliding beam experiments using vertex detection of beam-gas interactions*, *Nucl. Instrum. Meth. A* **553** (2005) 388 [[INSPIRE](#)].
- [30] LHCb collaboration, R. Aaij et al., *Absolute luminosity measurements with the LHCb detector at the LHC*, *2012 JINST* **7** P01010 [[arXiv:1110.2866](#)] [[INSPIRE](#)].
- [31] P. Golonka and Z. Was, *PHOTOS Monte Carlo: a precision tool for QED corrections in Z and W decays*, *Eur. Phys. J. C* **45** (2006) 97 [[hep-ph/0506026](#)] [[INSPIRE](#)].
- [32] A. Martin, W. Stirling, R. Thorne and G. Watt, *Parton distributions for the LHC*, *Eur. Phys. J. C* **63** (2009) 189 [[arXiv:0901.0002](#)] [[INSPIRE](#)].
- [33] S. Alekhin, J. Blumlein, S. Klein and S. Moch, *The 3, 4 and 5-flavor NNLO parton from deep-inelastic-scattering data and at hadron colliders*, *Phys. Rev. D* **81** (2010) 014032 [[arXiv:0908.2766](#)] [[INSPIRE](#)].
- [34] P. Jimenez-Delgado and E. Reya, *Dynamical NNLO parton distributions*, *Phys. Rev. D* **79** (2009) 074023 [[arXiv:0810.4274](#)] [[INSPIRE](#)].
- [35] R.D. Ball, L. Del Debbio, S. Forte, A. Guffanti, J.I. Latorre, et al., *A first unbiased global NLO determination of parton distributions and their uncertainties*, *Nucl. Phys. B* **838** (2010) 136 [[arXiv:1002.4407](#)] [[INSPIRE](#)].

The LHCb collaboration

R. Aaij³⁸, C. Abellan Beteta^{33,n}, A. Adametz¹¹, B. Adeva³⁴, M. Adinolfi⁴³, C. Adrover⁶, A. Affolder⁴⁹, Z. Ajaltouni⁵, J. Albrecht³⁵, F. Alessio³⁵, M. Alexander⁴⁸, S. Ali³⁸, G. Alkhazov²⁷, P. Alvarez Cartelle³⁴, A.A. Alves Jr²², S. Amato², Y. Amhis³⁶, J. Anderson³⁷, R.B. Appleby⁵¹, O. Aquines Gutierrez¹⁰, F. Archilli^{18,35}, A. Artamonov³², M. Artuso^{53,35}, E. Aslanides⁶, G. Auriemma^{22,m}, S. Bachmann¹¹, J.J. Back⁴⁵, V. Balagura^{28,35}, W. Baldini¹⁶, R.J. Barlow⁵¹, C. Barschel³⁵, S. Barsuk⁷, W. Barter⁴⁴, A. Bates⁴⁸, C. Bauer¹⁰, Th. Bauer³⁸, A. Bay³⁶, J. Beddow⁴⁸, I. Bediaga¹, S. Belogurov²⁸, K. Belous³², I. Belyaev²⁸, E. Ben-Haim⁸, M. Benayoun⁸, G. Bencivenni¹⁸, S. Benson⁴⁷, J. Benton⁴³, R. Bernet³⁷, M.-O. Bettler¹⁷, M. van Beuzekom³⁸, A. Bien¹¹, S. Bifani¹², T. Bird⁵¹, A. Bizzeti^{17,h}, P.M. Bjørnstad⁵¹, T. Blake³⁵, F. Blanc³⁶, C. Blanks⁵⁰, J. Blouw¹¹, S. Blusk⁵³, A. Bobrov³¹, V. Bocci²², A. Bondar³¹, N. Bondar²⁷, W. Bonivento¹⁵, S. Borghi^{48,51}, A. Borgia⁵³, T.J.V. Bowcock⁴⁹, C. Bozzi¹⁶, T. Brambach⁹, J. van den Brand³⁹, J. Bressieux³⁶, D. Brett⁵¹, M. Britsch¹⁰, T. Britton⁵³, N.H. Brook⁴³, H. Brown⁴⁹, A. Büchler-Germann³⁷, I. Burducea²⁶, A. Bursche³⁷, J. Buytaert³⁵, S. Cadeddu¹⁵, O. Callot⁷, M. Calvi^{20,j}, M. Calvo Gomez^{33,n}, A. Camboni³³, P. Campana^{18,35}, A. Carbone¹⁴, G. Carboni^{21,k}, R. Cardinale^{19,i,35}, A. Cardini¹⁵, L. Carson⁵⁰, K. Carvalho Akiba², G. Casse⁴⁹, M. Cattaneo³⁵, Ch. Cauet⁹, M. Charles⁵², Ph. Charpentier³⁵, N. Chiapolini³⁷, M. Chrzaszcz²³, K. Ciba³⁵, X. Cid Vidal³⁴, G. Ciezarek⁵⁰, P.E.L. Clarke⁴⁷, M. Clemencic³⁵, H.V. Cliff⁴⁴, J. Closier³⁵, C. Coca²⁶, V. Coco³⁸, J. Cogan⁶, E. Cogneras⁵, P. Collins³⁵, A. Comerma-Montells³³, A. Contu⁵², A. Cook⁴³, M. Coombes⁴³, G. Corti³⁵, B. Couturier³⁵, G.A. Cowan³⁶, R. Currie⁴⁷, C. D'Ambrosio³⁵, P. David⁸, P.N.Y. David³⁸, I. De Bonis⁴, K. De Bruyn³⁸, S. De Capua^{21,k}, M. De Cian³⁷, J.M. De Miranda¹, L. De Paula², P. De Simone¹⁸, D. Decamp⁴, M. Deckenhoff⁹, H. Degaudenzi^{36,35}, L. Del Buono⁸, C. Deplano¹⁵, D. Derkach^{14,35}, O. Deschamps⁵, F. Dettori³⁹, J. Dickens⁴⁴, H. Dijkstra³⁵, P. Diniz Batista¹, F. Domingo Bonal^{33,n}, S. Donleavy⁴⁹, F. Dordei¹¹, A. Dosil Suárez³⁴, D. Dossett⁴⁵, A. Dovbnya⁴⁰, F. Dupertuis³⁶, R. Dzhelyadin³², A. Dziurda²³, A. Dzyuba²⁷, S. Easo⁴⁶, U. Egede⁵⁰, V. Egorychev²⁸, S. Eidelman³¹, D. van Eijk³⁸, F. Eisele¹¹, S. Eisenhardt⁴⁷, R. Ekelhof⁹, L. Eklund⁴⁸, Ch. Elsasser³⁷, D. Elsby⁴², D. Esperante Pereira³⁴, A. Falabella^{16,e,14}, C. Färber¹¹, G. Fardell⁴⁷, C. Farinelli³⁸, S. Farry¹², V. Fave³⁶, V. Fernandez Albor³⁴, M. Ferro-Luzzi³⁵, S. Filippov³⁰, C. Fitzpatrick⁴⁷, M. Fontana¹⁰, F. Fontanelli^{19,i}, R. Forty³⁵, O. Francisco², M. Frank³⁵, C. Frei³⁵, M. Frosini^{17,f}, S. Furcas²⁰, A. Gallas Torreira³⁴, D. Galli^{14,c}, M. Gandelman², P. Gandini⁵², Y. Gao³, J.-C. Garnier³⁵, J. Garofoli⁵³, J. Garra Tico⁴⁴, L. Garrido³³, D. Gascon³³, C. Gaspar³⁵, R. Gauld⁵², N. Gauvin³⁶, M. Gersabeck³⁵, T. Gershon^{45,35}, Ph. Ghez⁴, V. Gibson⁴⁴, V.V. Gligorov³⁵, C. Göbel⁵⁴, D. Golubkov²⁸, A. Golutvin^{50,28,35}, A. Gomes², H. Gordon⁵², M. Grabalosa Gándara³³, R. Graciani Diaz³³, L.A. Granado Cardoso³⁵, E. Graugés³³, G. Graziani¹⁷, A. Grecu²⁶, E. Greening⁵², S. Gregson⁴⁴, O. Grünberg⁵⁵, B. Gui⁵³, E. Gushchin³⁰, Yu. Guz³², T. Gys³⁵, C. Hadjivasiliou⁵³, G. Haefeli³⁶, C. Haen³⁵, S.C. Haines⁴⁴, T. Hampson⁴³, S. Hansmann-Menzemer¹¹, N. Harnew⁵², J. Harrison⁵¹, P.F. Harrison⁴⁵, T. Hartmann⁵⁵, J. He⁷, V. Heijne³⁸, K. Hennessy⁴⁹, P. Henrard⁵,

J.A. Hernando Morata³⁴, E. van Herwijnen³⁵, E. Hicks⁴⁹, K. Holubyev¹¹, P. Hopchev⁴, W. Hulsbergen³⁸, P. Hunt⁵², T. Huse⁴⁹, R.S. Huston¹², D. Hutchcroft⁴⁹, D. Hynds⁴⁸, V. Iakovenko⁴¹, P. Ilten¹², J. Imong⁴³, R. Jacobsson³⁵, A. Jaeger¹¹, M. Jahjah Hussein⁵, E. Jans³⁸, F. Jansen³⁸, P. Jatou³⁶, B. Jean-Marie⁷, F. Jing³, M. John⁵², D. Johnson⁵², C.R. Jones⁴⁴, B. Jost³⁵, M. Kaballo⁹, S. Kandybei⁴⁰, M. Karacson³⁵, T.M. Karbach⁹, J. Keaveney¹², I.R. Kenyon⁴², U. Kerzel³⁵, T. Ketel³⁹, A. Keune³⁶, B. Khanji⁶, Y.M. Kim⁴⁷, M. Knecht³⁶, I. Komarov²⁹, R.F. Koopman³⁹, P. Koppenburg³⁸, M. Korolev²⁹, A. Kozlinskiy³⁸, L. Kravchuk³⁰, K. Kreplin¹¹, M. Kreps⁴⁵, G. Krocker¹¹, P. Krokovny³¹, F. Kruse⁹, K. Kruzelecki³⁵, M. Kucharczyk^{20,23,35,j}, V. Kudryavtsev³¹, T. Kvaratskheliya^{28,35}, V.N. La Thi³⁶, D. Lacarrere³⁵, G. Lafferty⁵¹, A. Lai¹⁵, D. Lambert⁴⁷, R.W. Lambert³⁹, E. Lanciotti³⁵, G. Lanfranchi¹⁸, C. Langenbruch³⁵, T. Latham⁴⁵, C. Lazzeroni⁴², R. Le Gac⁶, J. van Leerdam³⁸, J.-P. Lees⁴, R. Lefèvre⁵, A. Leflat^{29,35}, J. Lefrançois⁷, O. Leroy⁶, T. Lesiak²³, L. Li³, Y. Li³, L. Li Gioi⁵, M. Lieng⁹, M. Liles⁴⁹, R. Lindner³⁵, C. Linn¹¹, B. Liu³, G. Liu³⁵, J. von Loeben²⁰, J.H. Lopes², E. Lopez Asamar³³, N. Lopez-March³⁶, H. Lu³, J. Luisier³⁶, A. Mac Raighne⁴⁸, F. Machefert⁷, I.V. Machikhiliyan^{4,28}, F. Maciuc¹⁰, O. Maev^{27,35}, J. Magnin¹, S. Malde⁵², R.M.D. Mamunur³⁵, G. Manca^{15,d}, G. Mancinelli⁶, N. Mangiafave⁴⁴, U. Marconi¹⁴, R. Märki³⁶, J. Marks¹¹, G. Martellotti²², A. Martens⁸, L. Martin⁵², A. Martín Sánchez⁷, M. Martinelli³⁸, D. Martinez Santos³⁵, A. Massafferri¹, Z. Mathe¹², C. Matteuzzi²⁰, M. Matveev²⁷, E. Maurice⁶, B. Maynard⁵³, A. Mazurov^{16,30,35}, G. McGregor⁵¹, R. McNulty¹², M. Meissner¹¹, M. Merk³⁸, J. Merkel⁹, S. Miglioranzi³⁵, D.A. Milanese¹³, M.-N. Minard⁴, J. Molina Rodriguez⁵⁴, S. Monteil⁵, D. Moran¹², P. Morawski²³, R. Mountain⁵³, I. Mous³⁸, F. Muheim⁴⁷, K. Müller³⁷, R. Muresan²⁶, B. Muryn²⁴, B. Muster³⁶, J. Mylroie-Smith⁴⁹, P. Naik⁴³, T. Nakada³⁶, R. Nandakumar⁴⁶, I. Nasteva¹, M. Needham⁴⁷, N. Neufeld³⁵, A.D. Nguyen³⁶, C. Nguyen-Mau^{36,o}, M. Nicol⁷, V. Niess⁵, N. Nikitin²⁹, T. Nikodem¹¹, A. Nomerotski^{52,35}, A. Novoselov³², A. Oblakowska-Mucha²⁴, V. Obraztsov³², S. Oggero³⁸, S. Ogilvy⁴⁸, O. Okhrimenko⁴¹, R. Oldeman^{15,d,35}, M. Orlandea²⁶, J.M. Otalora Goicochea², P. Owen⁵⁰, B.K. Pal⁵³, J. Palacios³⁷, A. Palano^{13,b}, M. Palutan¹⁸, J. Panman³⁵, A. Papanestis⁴⁶, M. Pappagallo⁴⁸, C. Parkes⁵¹, C.J. Parkinson⁵⁰, G. Passaleva¹⁷, G.D. Patel⁴⁹, M. Patel⁵⁰, S.K. Paterson⁵⁰, G.N. Patrick⁴⁶, C. Patrignani^{19,i}, C. Pavel-Nicorescu²⁶, A. Pazos Alvarez³⁴, A. Pellegrino³⁸, G. Penso^{22,l}, M. Pepe Altarelli³⁵, S. Perazzini^{14,c}, D.L. Perego^{20,j}, E. Perez Trigo³⁴, A. Pérez-Calero Yzquierdo³³, P. Perret⁵, M. Perrin-Terrin⁶, G. Pessina²⁰, A. Petrolini^{19,i}, A. Phan⁵³, E. Picatoste Olloqui³³, B. Pie Valls³³, B. Pietrzyk⁴, T. Pilar⁴⁵, D. Pinci²², R. Plackett⁴⁸, S. Playfer⁴⁷, M. Plo Casasus³⁴, G. Polok²³, A. Poluektov^{45,31}, E. Polcarpo², D. Popov¹⁰, B. Popovici²⁶, C. Potterat³³, A. Powell⁵², J. Prisciandaro³⁶, V. Pugatch⁴¹, A. Puig Navarro³³, W. Qian⁵³, J.H. Rademacker⁴³, B. Rakotomiaramananana³⁶, M.S. Rangel², I. Raniuk⁴⁰, G. Raven³⁹, S. Redford⁵², M.M. Reid⁴⁵, A.C. dos Reis¹, S. Ricciardi⁴⁶, A. Richards⁵⁰, K. Rinnert⁴⁹, D.A. Roa Romero⁵, P. Robbe⁷, E. Rodrigues^{48,51}, F. Rodrigues², P. Rodriguez Perez³⁴, G.J. Rogers⁴⁴, S. Roiser³⁵, V. Romanovsky³², M. Rosello^{33,n}, J. Rouvinet³⁶, T. Ruf³⁵, H. Ruiz³³, G. Sabatino^{21,k}, J.J. Saborido Silva³⁴, N. Sagidova²⁷, P. Sail⁴⁸, B. Saitta^{15,d}, C. Salzmann³⁷, M. Sannino^{19,i}, R. Santacesaria²², C. Santamarina Rios³⁴, R. Santinelli³⁵, E. Santovetti^{21,k}, M. Sapunov⁶,

A. Sarti^{18,l}, C. Satriano^{22,m}, A. Satta²¹, M. Savrie^{16,e}, D. Savrina²⁸, P. Schaack⁵⁰, M. Schiller³⁹, H. Schindler³⁵, S. Schleich⁹, M. Schlupp⁹, M. Schmelling¹⁰, B. Schmidt³⁵, O. Schneider³⁶, A. Schopper³⁵, M.-H. Schune⁷, R. Schwemmer³⁵, B. Sciascia¹⁸, A. Sciubba^{18,l}, M. Seco³⁴, A. Semennikov²⁸, K. Senderowska²⁴, I. Sepp⁵⁰, N. Serra³⁷, J. Serrano⁶, P. Seyfert¹¹, M. Shapkin³², I. Shapoval^{40,35}, P. Shatalov²⁸, Y. Shcheglov²⁷, T. Shears⁴⁹, L. Shekhtman³¹, O. Shevchenko⁴⁰, V. Shevchenko²⁸, A. Shires⁵⁰, R. Silva Coutinho⁴⁵, T. Skwarnicki⁵³, N.A. Smith⁴⁹, E. Smith^{52,46}, M. Smith⁵¹, K. Sobczak⁵, F.J.P. Soler⁴⁸, A. Solomin⁴³, F. Soomro^{18,35}, B. Souza De Paula², B. Spaan⁹, A. Sparkes⁴⁷, P. Spradlin⁴⁸, F. Stagni³⁵, S. Stahl¹¹, O. Steinkamp³⁷, S. Stoica²⁶, S. Stone^{53,35}, B. Storaci³⁸, M. Straticiuc²⁶, U. Straumann³⁷, V.K. Subbiah³⁵, S. Swientek⁹, M. Szczekowski²⁵, P. Szczypka³⁶, T. Szumlak²⁴, S. T’Jampens⁴, E. Teodorescu²⁶, F. Teubert³⁵, C. Thomas⁵², E. Thomas³⁵, J. van Tilburg¹¹, V. Tisserand⁴, M. Tobin³⁷, S. Tolk³⁹, S. Topp-Joergensen⁵², N. Torr⁵², E. Tournefier^{4,50}, S. Tourneur³⁶, M.T. Tran³⁶, A. Tsaregorodtsev⁶, N. Tuning³⁸, M. Ubeda Garcia³⁵, A. Ukleja²⁵, U. Uwer¹¹, V. Vagnoni¹⁴, G. Valenti¹⁴, R. Vazquez Gomez³³, P. Vazquez Regueiro³⁴, S. Vecchi¹⁶, J.J. Velthuis⁴³, M. Veltri^{17,g}, B. Viaud⁷, I. Videau⁷, D. Vieira², X. Vilasis-Cardona^{33,n}, J. Visniakov³⁴, A. Vollhardt³⁷, D. Volyanskyy¹⁰, D. Voong⁴³, A. Vorobyev²⁷, V. Vorobyev³¹, C. Voß⁵⁵, H. Voss¹⁰, R. Waldi⁵⁵, R. Wallace¹², S. Wandernoth¹¹, J. Wang⁵³, D.R. Ward⁴⁴, N.K. Watson⁴², A.D. Webber⁵¹, D. Websdale⁵⁰, M. Whitehead⁴⁵, J. Wicht³⁵, D. Wiedner¹¹, L. Wiggers³⁸, G. Wilkinson⁵², M.P. Williams^{45,46}, M. Williams⁵⁰, F.F. Wilson⁴⁶, J. Wishahi⁹, M. Witek²³, W. Witzeling³⁵, S.A. Wotton⁴⁴, S. Wright⁴⁴, S. Wu³, K. Wyllie³⁵, Y. Xie⁴⁷, F. Xing⁵², Z. Xing⁵³, Z. Yang³, R. Young⁴⁷, X. Yuan³, O. Yushchenko³², M. Zangoli¹⁴, M. Zavertyaev^{10,a}, F. Zhang³, L. Zhang⁵³, W.C. Zhang¹², Y. Zhang³, A. Zhelezov¹¹, L. Zhong³, A. Zvyagin³⁵.

¹Centro Brasileiro de Pesquisas Físicas (CBPF), Rio de Janeiro, Brazil

²Universidade Federal do Rio de Janeiro (UFRJ), Rio de Janeiro, Brazil

³Center for High Energy Physics, Tsinghua University, Beijing, China

⁴LAPP, Université de Savoie, CNRS/IN2P3, Annecy-Le-Vieux, France

⁵Clermont Université, Université Blaise Pascal, CNRS/IN2P3, LPC, Clermont-Ferrand, France

⁶CPPM, Aix-Marseille Université, CNRS/IN2P3, Marseille, France

⁷LAL, Université Paris-Sud, CNRS/IN2P3, Orsay, France

⁸LPNHE, Université Pierre et Marie Curie, Université Paris Diderot, CNRS/IN2P3, Paris, France

⁹Fakultät Physik, Technische Universität Dortmund, Dortmund, Germany

¹⁰Max-Planck-Institut für Kernphysik (MPIK), Heidelberg, Germany

¹¹Physikalisches Institut, Ruprecht-Karls-Universität Heidelberg, Heidelberg, Germany

¹²School of Physics, University College Dublin, Dublin, Ireland

¹³Sezione INFN di Bari, Bari, Italy

¹⁴Sezione INFN di Bologna, Bologna, Italy

¹⁵Sezione INFN di Cagliari, Cagliari, Italy

¹⁶Sezione INFN di Ferrara, Ferrara, Italy

¹⁷Sezione INFN di Firenze, Firenze, Italy

¹⁸Laboratori Nazionali dell’INFN di Frascati, Frascati, Italy

¹⁹Sezione INFN di Genova, Genova, Italy

²⁰Sezione INFN di Milano Bicocca, Milano, Italy

²¹Sezione INFN di Roma Tor Vergata, Roma, Italy

²²Sezione INFN di Roma La Sapienza, Roma, Italy

²³Henryk Niewodniczanski Institute of Nuclear Physics Polish Academy of Sciences, Kraków, Poland

- ²⁴AGH University of Science and Technology, Kraków, Poland
- ²⁵Soltan Institute for Nuclear Studies, Warsaw, Poland
- ²⁶Horia Hulubei National Institute of Physics and Nuclear Engineering, Bucharest-Magurele, Romania
- ²⁷Petersburg Nuclear Physics Institute (PNPI), Gatchina, Russia
- ²⁸Institute of Theoretical and Experimental Physics (ITEP), Moscow, Russia
- ²⁹Institute of Nuclear Physics, Moscow State University (SINP MSU), Moscow, Russia
- ³⁰Institute for Nuclear Research of the Russian Academy of Sciences (INR RAN), Moscow, Russia
- ³¹Budker Institute of Nuclear Physics (SB RAS) and Novosibirsk State University, Novosibirsk, Russia
- ³²Institute for High Energy Physics (IHEP), Protvino, Russia
- ³³Universitat de Barcelona, Barcelona, Spain
- ³⁴Universidad de Santiago de Compostela, Santiago de Compostela, Spain
- ³⁵European Organization for Nuclear Research (CERN), Geneva, Switzerland
- ³⁶Ecole Polytechnique Fédérale de Lausanne (EPFL), Lausanne, Switzerland
- ³⁷Physik-Institut, Universität Zürich, Zürich, Switzerland
- ³⁸Nikhef National Institute for Subatomic Physics, Amsterdam, The Netherlands
- ³⁹Nikhef National Institute for Subatomic Physics and VU University Amsterdam, Amsterdam, The Netherlands
- ⁴⁰NSC Kharkiv Institute of Physics and Technology (NSC KIPT), Kharkiv, Ukraine
- ⁴¹Institute for Nuclear Research of the National Academy of Sciences (KINR), Kyiv, Ukraine
- ⁴²University of Birmingham, Birmingham, United Kingdom
- ⁴³H.H. Wills Physics Laboratory, University of Bristol, Bristol, United Kingdom
- ⁴⁴Cavendish Laboratory, University of Cambridge, Cambridge, United Kingdom
- ⁴⁵Department of Physics, University of Warwick, Coventry, United Kingdom
- ⁴⁶STFC Rutherford Appleton Laboratory, Didcot, United Kingdom
- ⁴⁷School of Physics and Astronomy, University of Edinburgh, Edinburgh, United Kingdom
- ⁴⁸School of Physics and Astronomy, University of Glasgow, Glasgow, United Kingdom
- ⁴⁹Oliver Lodge Laboratory, University of Liverpool, Liverpool, United Kingdom
- ⁵⁰Imperial College London, London, United Kingdom
- ⁵¹School of Physics and Astronomy, University of Manchester, Manchester, United Kingdom
- ⁵²Department of Physics, University of Oxford, Oxford, United Kingdom
- ⁵³Syracuse University, Syracuse, NY, United States
- ⁵⁴Pontifícia Universidade Católica do Rio de Janeiro (PUC-Rio), Rio de Janeiro, Brazil, associated to ²
- ⁵⁵Institut für Physik, Universität Rostock, Rostock, Germany, associated to ¹¹

^aP.N. Lebedev Physical Institute, Russian Academy of Science (LPI RAS), Moscow, Russia

^bUniversità di Bari, Bari, Italy

^cUniversità di Bologna, Bologna, Italy

^dUniversità di Cagliari, Cagliari, Italy

^eUniversità di Ferrara, Ferrara, Italy

^fUniversità di Firenze, Firenze, Italy

^gUniversità di Urbino, Urbino, Italy

^hUniversità di Modena e Reggio Emilia, Modena, Italy

ⁱUniversità di Genova, Genova, Italy

^jUniversità di Milano Bicocca, Milano, Italy

^kUniversità di Roma Tor Vergata, Roma, Italy

^lUniversità di Roma La Sapienza, Roma, Italy

^mUniversità della Basilicata, Potenza, Italy

ⁿLIFAELS, La Salle, Universitat Ramon Llull, Barcelona, Spain

^oHanoi University of Science, Hanoi, Viet Nam